The Astrophysical Journal Supplement Series, 255:23 (18pp), 2021 August https://doi.org/10.3847/1538-4365/ac0bb5

Deuterated Polycyclic Aromatic Hydrocarbons in the Interstellar Medium: The C–D Band Strengths of Multideuterated Species

X. J. Yang[1,2], Aigen Li[2], C. Y. He[3], and R. Glaser[4]
[1] Hunan Key Laboratory for Stellar and Interstellar Physics and School of Physics and Optoelectronics, Xiangtan University, Hunan 411105, People's Republic of China; xjyang@xtu.edu.cn
[2] Department of Physics and Astronomy, University of Missouri, Columbia, MO 65211, USA; lia@missouri.edu
[3] Hunan Key Laboratory for Micro-Nano Energy Materials and Devices and School of Physics and Optoelectronics, Xiangtan University, Hunan 411105, People's Republic of China
[4] Department of Chemistry, Missouri University of Science and Technology, Rolla, MO 65409, USA
Received 2021 March 8; revised 2021 June 6; accepted 2021 June 14; published 2021 July 28

Abstract

Observationally, the interstellar gas-phase abundance of deuterium (D) is considerably depleted and the missing D atoms are often postulated to have been locked up into carbonaceous solids and polycyclic aromatic hydrocarbon (PAH) molecules. An accurate knowledge of the fractional amount of D (relative to H) tied up in carbon dust and PAHs has important cosmological implications since D originated exclusively from the Big Bang and the present-day D abundance, after accounting for the astration it has experienced during Galactic evolution, provides essential clues to the primordial nucleosynthesis and the cosmological parameters. To quantitatively explore the extent to which PAHs could possibly accommodate the observed D depletion, we have previously quantum-chemically computed the infrared vibrational spectra of *monodeuterated* PAHs and derived the mean intrinsic band strengths of the 3.3 μm C–H stretch ($A_{3.3}$) and the 4.4 μm C–D stretch ($A_{4.4}$). Here we extend our previous work to *multideuterated* PAH species of different deuterations, sizes, and structures. We find that both the intrinsic band strengths $A_{3.3}$ and $A_{4.4}$ (on a per-unit-bond basis) and their ratios $A_{4.4}/A_{3.3}$ not only show little variation among PAHs of different deuterations, sizes, and structures, they are also closely similar to that of monodeuterated PAHs. Therefore, a PAH deuteration level (i.e., the fraction of peripheral atoms attached to C atoms in the form of D) of $\sim$2.4% previously estimated from the observed 4.4 to 3.3 μm band ratio based on the $A_{4.4}/A_{3.3}$ ratio of monodeuterated PAHs is robust.

Unified Astronomy Thesaurus concepts: Polycyclic aromatic hydrocarbons (1280); Interstellar line emission (844); Line intensities (2084); Astrochemistry (75); Interstellar molecules (849)

1. Introduction

The interstellar abundance of deuterium (D) provides important insights into the Big Bang cosmology. Exclusively created in the Big Bang, the primordial abundance of D depends sensitively on the cosmological parameters such as the baryon closure parameter Ω_b and the Hubble constant h (see Boesgaard & Steigman 1985). The standard Big Bang nucleosynthesis (BBN) model predicts a primordial D/H abundance of $[D/H]_{prim} \approx 26$ ppm from the Ω_b and h parameters derived from observations of the cosmic microwave background (e.g., see Spergel et al. 2003; Coc et al. 2004; Sánchez et al. 2006). This is closely consistent with the observationally determined abundance of $[D/H]_{prim} \approx$ 25–28 ppm, based on high-precision measurements of the column densities of D I and H I of compositionally "pristine" metal-poor quasar absorption line systems and damped Lyα absorption systems (e.g., see Cooke et al. 2018; Zavarygin et al. 2018).

Once incorporated into stars, deuterium could be easily destroyed by nuclear fusion in stellar interiors, a process known as "astration" which converts D to ^{3}He, ^{4}He, and heavier elements. Conventional Galactic chemical evolution models predict a monotonic decrease in D/H with time (Mazzitelli & Moretti 1980), with a present-day D/H abundance of $[D/H]_{ISM} \gtrsim 20 \pm 1$ ppm in the Galactic interstellar medium (ISM; see Prodanović et al. 2010). However, high-resolution ultraviolet (UV) spectroscopic observations of the local ISM have revealed that the interstellar gas-phase $[D/H]_{gas}$ abundance exhibits substantial regional variations (by a factor of $\sim$4) within a few hundred parsecs of the Sun, with some lines of sight exhibiting a much lower gas-phase D/H abundance than the expected interstellar D/H abundance of $[D/H]_{ISM} \gtrsim 20 \pm 1$ ppm (see Draine 2006 and references therein).[5]

The puzzling underabundance of the gas-phase $[D/H]_{gas}$ abundance (in comparison with the present-epoch interstellar D/H abundance of $[D/H]_{ISM} \gtrsim 20 \pm 1$ ppm expected from the BBN model and the Galactic chemical evolution model) and the apparent regional variations of $[D/H]_{gas}$ could be related to carbonaceous solids and polycyclic aromatic hydrocarbon (PAH) molecules. More specifically, Draine (2004) proposed that D might be depleted from the gas phase and sequestered in PAHs. The variations in the gas-phase $[D/H]_{gas}$ abundance could be attributed to variations from one sight line to another in the fraction of the D atoms sequestered in PAHs. Many processes have been proposed to drive deuterium enrichment in PAHs (see Sandford et al. 2001). Due to the lower zero-point energy of C–D bonds (in comparison with C–H bonds), PAHs of intermediate size are expected to become deuterium enriched in the ISM through the selective loss of hydrogen during photodissociation events (Allamandola et al. 1989). Draine (2006) also showed that collisions of D with PAH cations and D^+ with PAHs could incorporate D into PAHs and efficiently deplete D from the gas on timescales of $\sim$2 Myr in cool diffuse

[5] Using the UV absorption spectra obtained with the Copernicus satellite, Allen et al. (1992) derived $[D/H]_{gas} = 5.0 \pm 1.6$ ppm toward θ Car at a distance of $d = 135 \pm 9$ pc. Jenkins et al. (1999) measured $[D/H]_{gas} = 7.4^{+1.2}_{-0.9}$ ppm toward δ Ori ($d = 281 \pm 65$ pc), based on the Lyδ and Lyε absorption features of D obtained with the Interstellar Medium Absorption Profile Spectrograph on the ORFEUS-SPAS II mission.

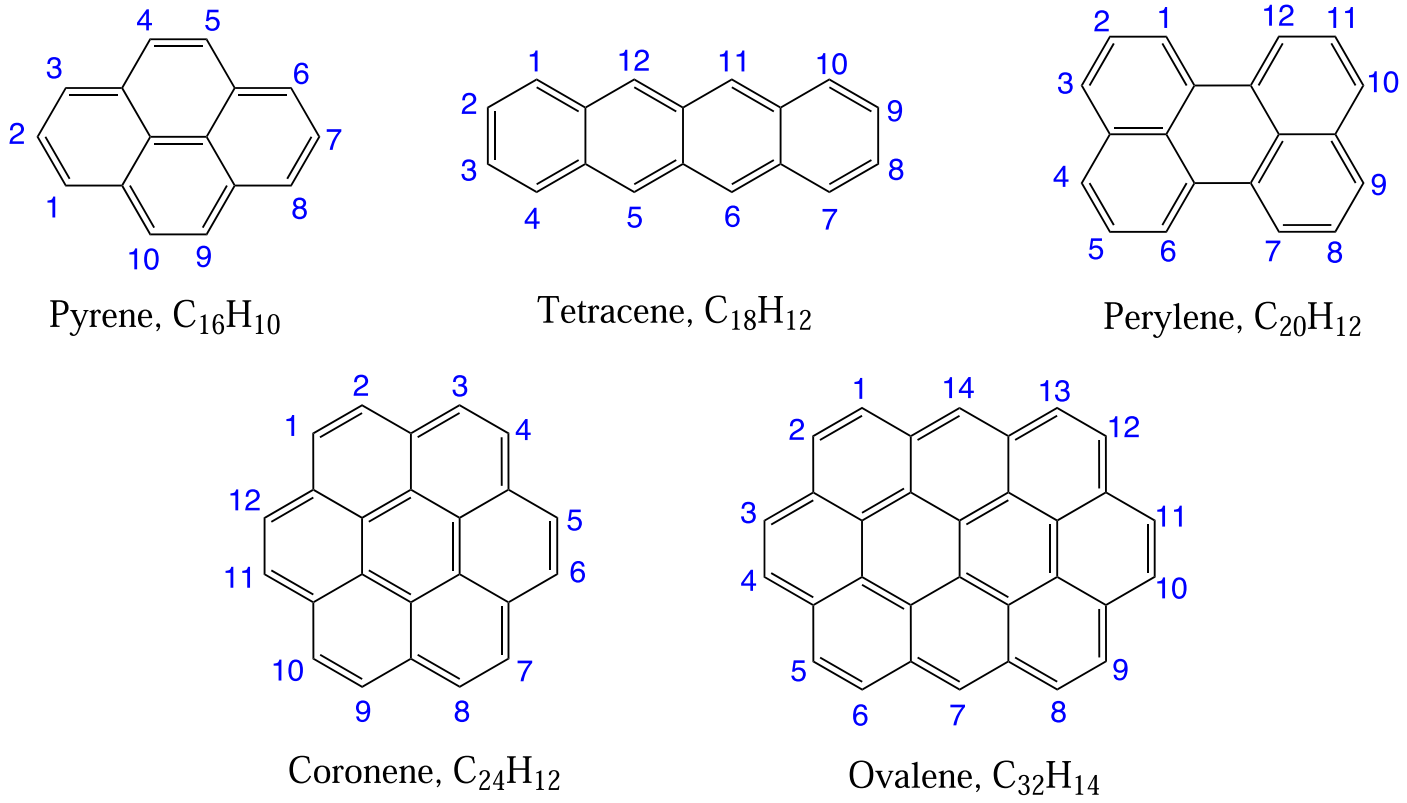

Figure 1. Structures of parent PAHs considered here for deuteration. For a multideuterated species, we refer it by the abbreviation of the first four letters of the name of its parental molecule, followed by the number of D atoms attached (e.g., Pyre_2D refers to doubly deuterated pyrene).

clouds. Bernstein et al. (1999) and Sandford et al. (2000) have demonstrated experimentally that UV photolysis of PAHs in D-enriched ices could result in rapid D enrichment and even produce multideuterated PAHs. The latter process is particularly relevant for dense regions where ices are photochemically processed by ambient UV photons. Deuterium enrichment of extraterrestrial organic compounds has been experimentally measured, including aromatics in meteorites and interplanetary dust particles (Allamandola et al. 1987; Kerridge et al. 1987; Clemett et al. 1993). Indeed, PAHs represent a major carrier of D excesses in primitive meteorites (Kerridge et al. 1987).

PAHs are abundant and widespread throughout the universe, as revealed by their distinctive set of infrared (IR) emission bands at 3.3, 6.2, 7.7, 8.6, 11.3, and 12.7 μm, which are characteristic of their C–H and C–C vibrational modes and are often also known as the "unidentified infrared emission" (UIE) bands (see Li 2020).[6] Upon deuteration (i.e., one or more peripheral H atoms are replaced by D), additional bands at $\sim$4.4 μm (C–D stretching), $\sim$11.7 μm (C–D in-plane bending), and $\sim$15.4 μm (C–D out-of-plane [oop] bending) are expected to show up in their emission spectra (see Hudgins et al. 1994, 2004; Bauschlicher et al. 1997; Draine 2006; Yang et al. 2020b). While the 11.7 μm C–D band might be confused with the C–H oop bending modes at $\sim$11.3 μm and the 15.4 μm C–D band falls in a region where various weak C–C skeleton modes are present, the 4.4 μm C–D band appears to be the best probe of the deuteration of interstellar PAHs. Indeed, a weak band at 4.4 μm has been detected by the Infrared Space Observatory and AKARI in photodissociated regions, reflection nebulae, and H II regions in both the Milky Way and Large and Small Magellanic Clouds (Peeters et al. 2004; Onaka et al. 2014; Doney et al. 2016). Meanwhile, a weak band at 4.65 μm was also detected in these regions, which is generally attributed to emission from the aliphatic C–D stretch.

To quantitatively explore the hypothesis of PAHs as a possible reservoir of interstellar D, we have previously performed quantum-chemical computations on the IR vibrational spectra of *monodeuterated* PAHs of various sizes and determined the intrinsic band strength of the 4.4 μm C–D stretch. By comparing the computed 4.4 μm C–D band strength with the observed intensities, we have derived the degree of deuteration (i.e., the fraction of peripheral atoms attached to C atoms in the form of D) to be $\sim$2.4%, implying that interstellar PAHs could be D-enriched by a factor of $[D/H]_{PAH}/[D/H]_{ISM} \approx 1200$ (Yang et al. 2020b). However, it is not impossible that some PAHs may be *multideuterated* in the ISM, i.e., two or more peripheral H atoms are replaced by D atoms. The detection of various multiply deuterated gas-phase species in dense clouds such as D_2CO (Loinard et al. 2000), NHD_2 and ND_3 (Roueff et al. 2000; van der Tak et al. 2002), CHD_2OH (Parise et al. 2002), and D_2S (Vastel et al. 2003) indicates that multiple deuteration may also occur in interstellar PAHs. To explore the photochemistry of small PAHs in ices under interstellar conditions, Bernstein et al. (1999) and

[6] In astronomy, "PAH" is a generic term. To fit the observed astronomical UIE spectra, the PAH model requires a mixture of *specific* PAH molecules (e.g., see Cami 2011; Rosenberg et al. 2011) or empirical "astro-PAHs" (Li & Draine 2001; Draine & Li 2007; Draine et al. 2020) of various sizes and charging states (i.e., neutrals, cations, and anions). No specific PAH molecules have been identified in space until very recently McGuire et al. (2021) reported the first detection of two isomers of cyanonapthalene ($C_{11}H_7N$), a bicyclic ring molecule, in the TMC-1 molecular cloud. Alternatively, other carriers have also been proposed for the UIE bands (e.g., see Kwok & Zhang 2011; Zhang & Kwok 2015; Bernstein et al. 2017; Sadjadi et al. 2017).

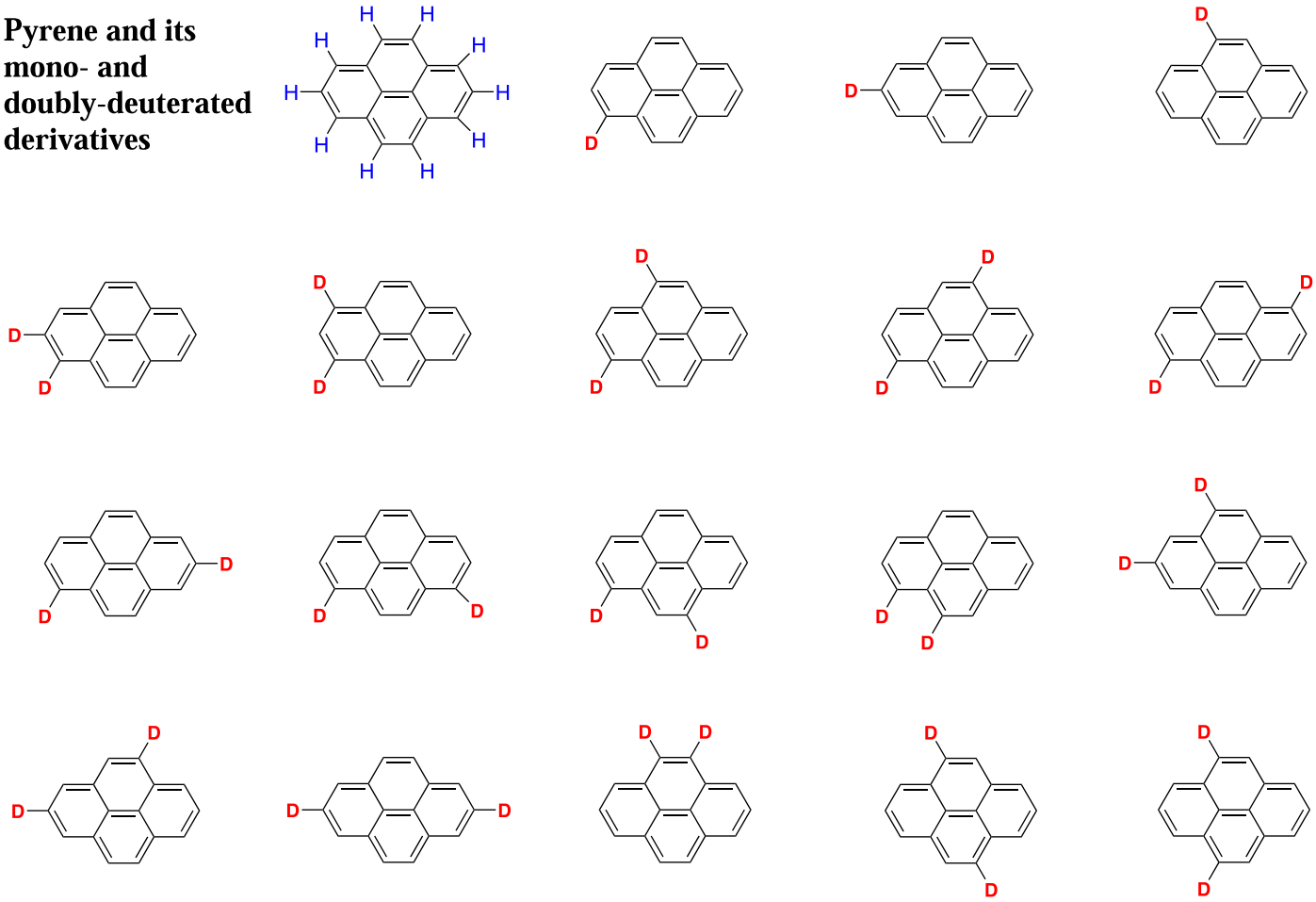

Figure 2. Structures of pyrene ($C_{16}H_{10}$) and its three monodeuterated isomers (Pyre_1D) and 15 dideuterated isomers (Pyre_2D).

Sandford et al. (2000) applied UV irradiation to PAH-containing D-rich ices and found that UV photolysis of PAHs in low-temperature ices could easily cause one or more of the peripheral H atoms on PAHs to be replaced by D atoms. These deuterated and multideuterated PAHs created in dense clouds could be present in the diffuse ISM through rapid exchange of material between diffuse and dense clouds.[7]

To complement our previous work on monodeuterated PAHs, in this work we focus on multideuterated species, aiming at deriving the intrinsic band strength of the 4.4 μm C–D stretch of multideuterated PAHs and comparing it with that of monodeuterated species. To this end, we perform quantum-chemical computations on the IR vibrational spectra of a large sample of multideuterated molecules. This paper is organized as follows. In Section 2 we briefly describe the computational methods and the selected target molecules. The computed IR vibrational spectra and the derived intrinsic C–D band strengths are reported in Section 3. In Section 4 we present the recommended C–D band strengths and discuss the astrophysical implications. Finally, we summarize our major results in Section 5.

2. Computational Methods and Target Molecules

We use the Gaussian16 software (Frisch et al. 2016) to calculate the vibrational spectra for a large number of multiply deuterated species of five parental molecules (see Figure 1): pyrene ($C_{16}H_{10}$), tetracene ($C_{18}H_{12}$), perylene ($C_{20}H_{12}$), coronene ($C_{24}H_{12}$), and ovalene ($C_{32}H_{14}$). Our target molecules are mostly compact and pericondensed (i.e., pyrene, perylene, coronene, and ovalene). For comparison, we also consider one linear, catacondensed molecule (i.e., tetracene). Larger PAHs of more than 40 carbon atoms (i.e., $N_C \gtrsim 40$) are less likely to be deuterated (see Hudgins et al. 2004) since they have a large number of internal degrees of freedom to accommodate the absorbed photon energy and hence peripheral C–H bond rupture does not occur.

For each parent PAH molecule, we consider all deuteration possibilities, from monodeuteration[8] all the way up to complete deuteration or perdeuteration.[9] We assume that all the D atoms are attached to the aromatic C atoms, although both astronomical observations and UV irradiation of PAHs in interstellar ice analogs have suggested that D could also be attached to aliphatic C atoms (Bernstein et al. 1999; Sandford et al. 2000, 2001;

[7] It is well recognized that in the diffuse ISM, dust grains (e.g., silicate and graphite) are destroyed at a rate faster than their stellar production (McKee 1989). This led Draine (1990) to conclude that the bulk of the solid material in grains actually condensed in the ISM rather than in stellar outflows. Draine (1990) argued that there must be rapid exchange of matter between the diffuse ISM and molecular clouds on a timescale of $\sim 2 \times 10^7$ yr or less since the bulk of grain growth can proceed rapidly only in dense regions.

[8] For completeness, the band strengths computed for monodeuterated species reported in Yang et al. (2020b) are also included here when we derive the mean band strengths for all isomers. Note that monodeuterated isomers are only a minor fraction of our target sample. The inclusion or exclusion of monodeuterated isomers does not essentially affect our results.

[9] Perdeuterated PAHs refer to PAHs in which all of the peripheral H atoms have been replaced by D atoms.

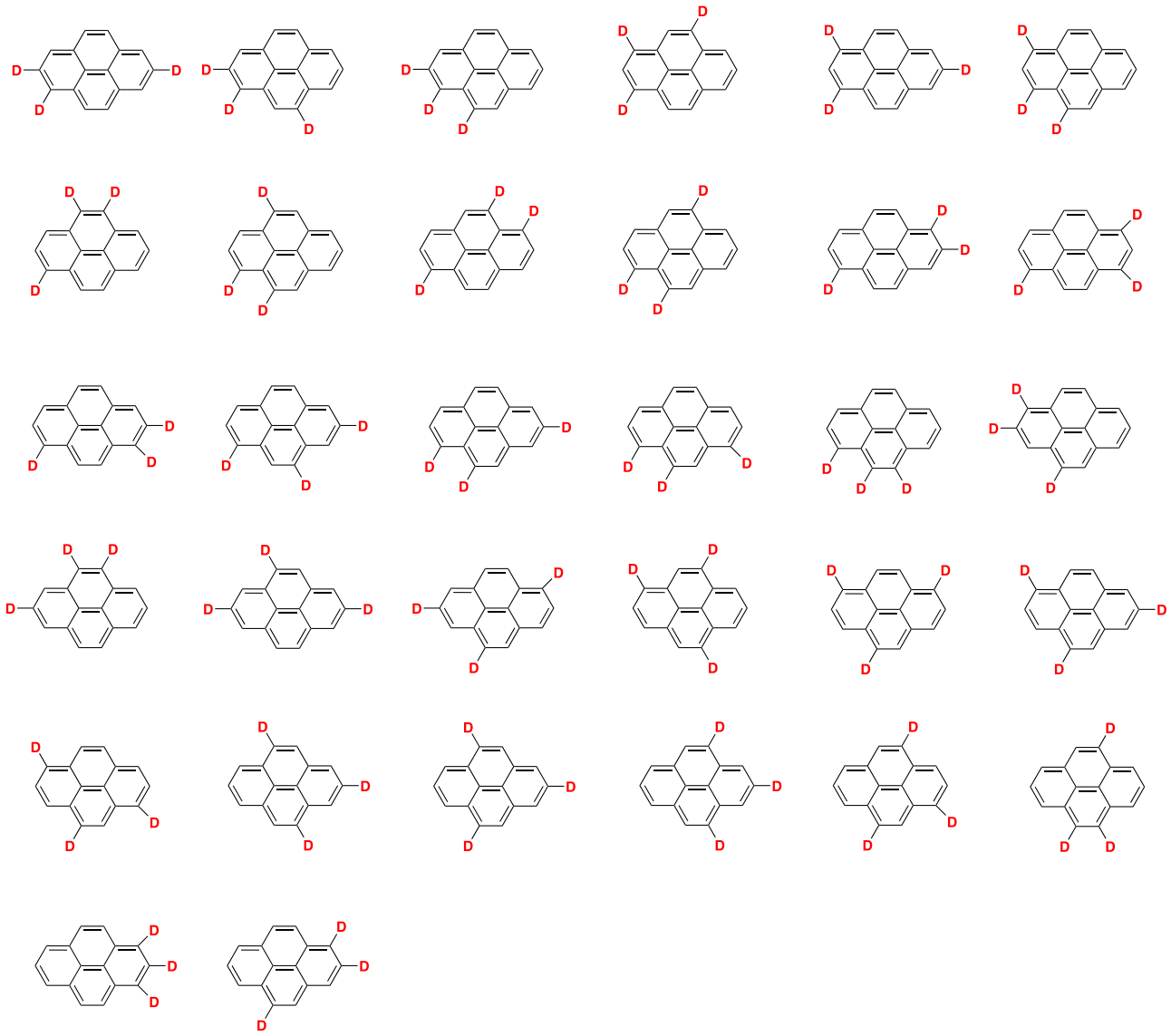

Figure 3. Structures of the 32 isomers considered for triply deuterated pyrenes (Pyre_3D).

Peeters et al. 2004; Onaka et al. 2014; Buragohain et al. 2015, 2016, 2020; Doney et al. 2016).

Similar to Yang et al. (2020b), we refer monodeuterated species by the abbreviation of the first four letters of the names of their parental PAH molecules followed by the position where the D atom is attached (e.g., Pyre_D2 refers to monodeuterated pyrene in which the (only) D atom is attached at position 2). For multiply deuterated species, we also refer them by the abbreviation of the first four letters of the names of their parental molecules, but followed by the number of D atoms attached (e.g., Pyre_2D refers to dideuterated pyrene). For each multideuterated molecule (of the same degree of deuteration), depending on the positioning of the D atoms, there are many isomers (e.g., Pyre_2D has 15 isomers; see Figure 2).[10] In naming, we do not further distinguish these isomers. We do distinguish them when we compute their vibrational spectra (see Section 3).

Following Yang et al. (2020b), the hybrid density functional theoretical (DFT) method (B3LYP) at the 6-311+G** level is employed for the calculation of IR vibrational spectra under the harmonic approximation, which provides sufficient computational accuracies with operable computer time (see Yang et al. 2017 and references therein). We present the harmonic vibrational frequencies and intensities, with the standard scaling applied to the frequencies by employing a scale factor of ∼0.9688 (Borowski 2012).

3. Results

3.1. Theoretical Background and Precomputational Expectations

The B3LYP DFT computational technique adopted in this work is based on the Born–Oppenheimer (BO) approximation, a simplified description of the quantum states of molecules which separates the motion of the nuclei and the motion of the

[10] Consider a PAH molecule consisting of x carbon atoms and y hydrogen atoms (i.e., C_xH_y). With z peripheral H atoms replaced by D atoms, it is deuterated into $C_xH_{y-z}D_z$. For each configuration of C_xH_y, there are in total 2^y isomers for $C_xH_{y-z}D_z$, according to the principle of permutation and combination. However, a large fraction of these isomers are equivalent due to symmetry. In this work, to avoid duplicate isomers, we will confine ourselves to those "inequivalent" isomers given by the RG2 code (Shi et al. 2018).

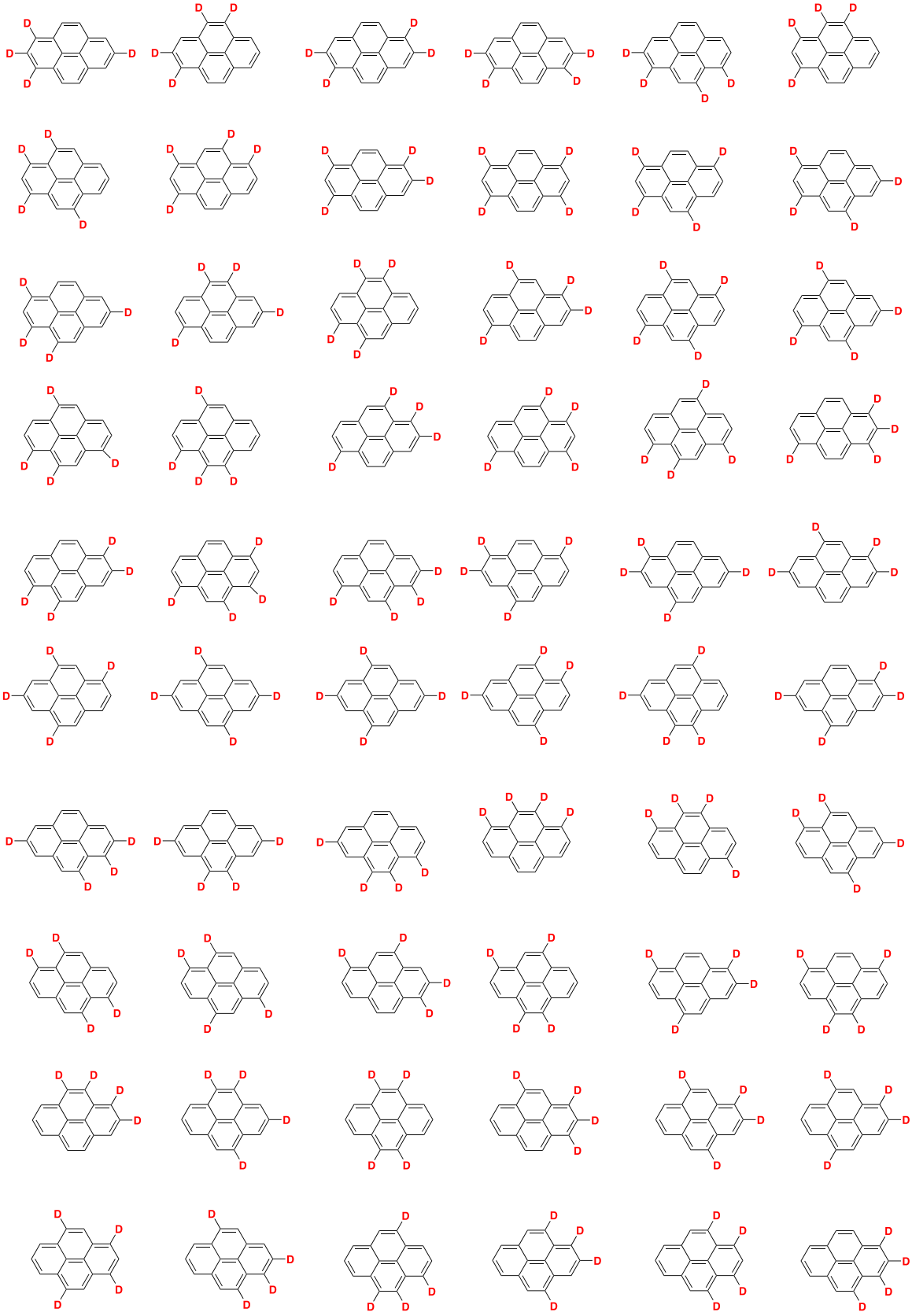

Figure 4. Structures of the 60 isomers considered for quartet-deuterated pyrenes (Pyre_4D).

electrons. The physical basis for the BO approximation is the fact that the mass of an atomic nucleus in a molecule is much larger (by over 1000 times) than the mass of an electron. Because of this mass difference, the nuclei move much more slowly than the electrons, and the electrons adjust instantaneously to any nuclear motion.

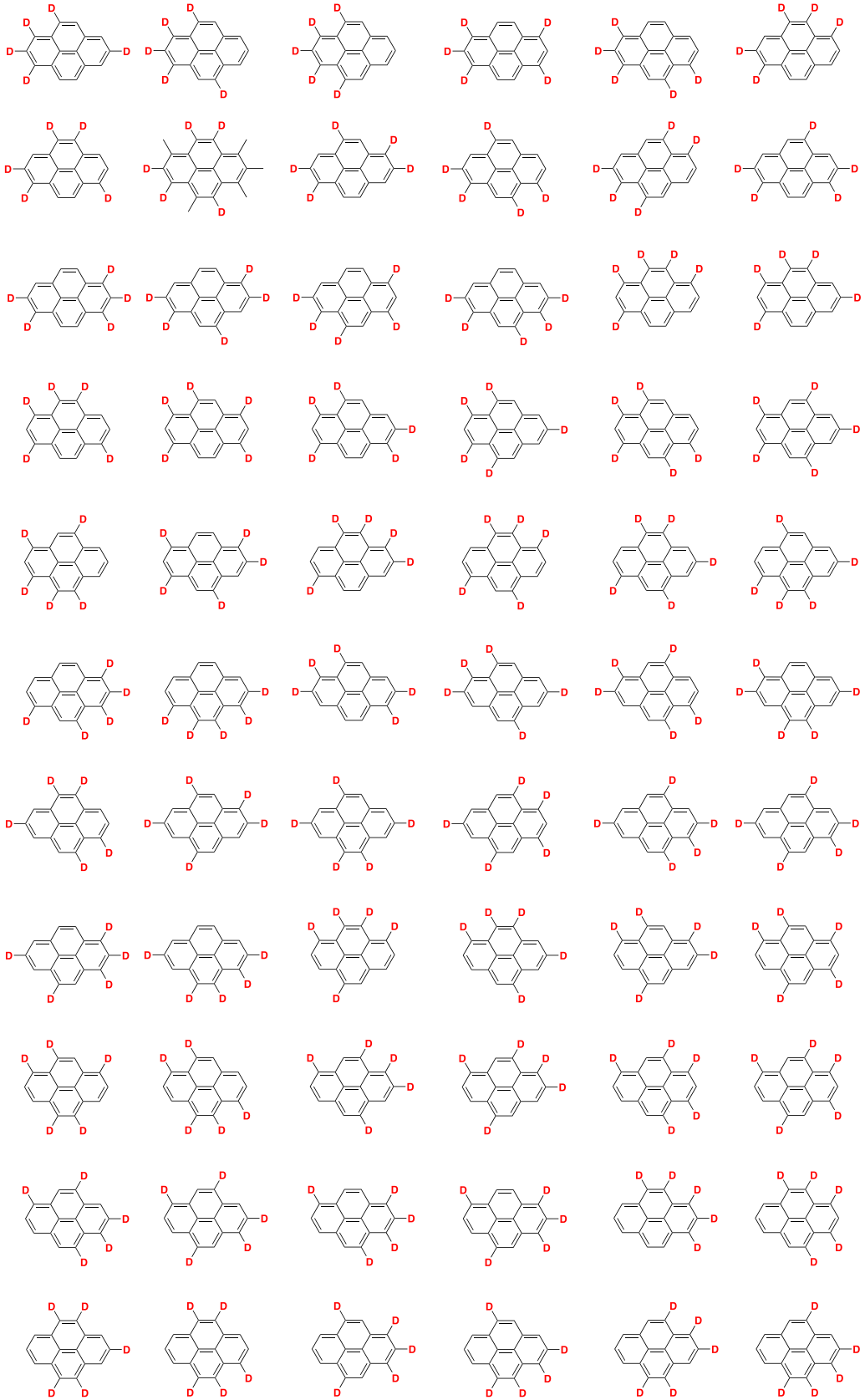

Figure 5. Structures of the 66 isomers considered for quintet-deuterated pyrenes (Pyre_5D).

In the harmonic approximation, the vibrational frequency of a chemical bond can be estimated from $\nu = \sqrt{k/\mu}/2\pi$, where μ is the reduced mass, and k, the force constant, is the second derivative of the potential energy V, $k = \partial^2 V/\partial Q^2$, where Q is the vibrational normal coordinate. The vibrational band intensity A is related to electron charge displacements (i.e.,

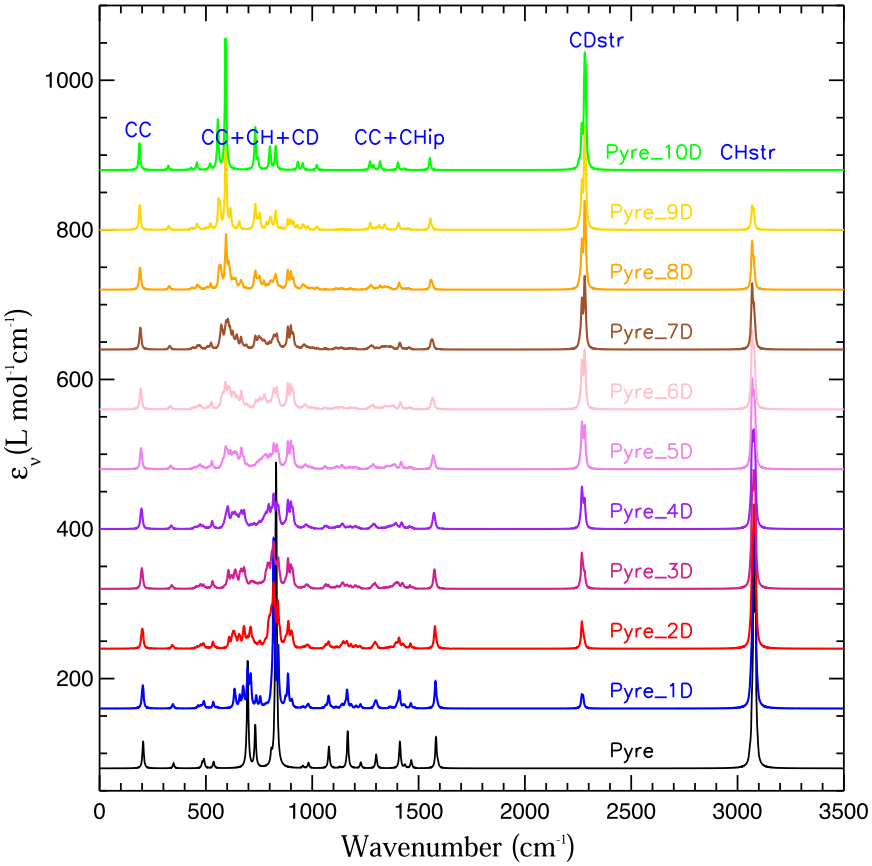

Figure 6. DFT-computed vibrational absorption spectra of deuterated pyrenes of all possible deuterations, from zero-deuteration (i.e., pure pyrene $C_{16}H_{10}$), monodeuteration (Pyre_1D, $C_{16}H_9D$), dideuteration (Pyre_2D, $C_{16}H_8D_2$), all the way to perdeuteration (Pyre_10D, $C_{16}D_{10}$). For each deuteration, the spectrum is obtained by averaging over all the considered isomers. The frequencies are scaled with a factor of 0.9688, and a line width of 4 cm^{-1} is assigned. For perdeuterated pyrene, as expected, the 3.3 μm C–H stretch is absent in the computed spectra due to the lack of H atoms in perdeuterated species.

changes in the dipole moment vector $\vec{\mu}$ with vibrational coordinate) occurring in a chemical bond over the lifetime of a vibration, $A \propto |\partial\vec{\mu}/\partial Q|^2$ (see Wexler 1967). Under the BO approximation, the presence of D atoms only affects the reduced mass μ and barely affects the force constants k and the dipole moment derivatives $\partial\vec{\mu}/\partial Q$. Therefore, one would expect that the frequency and intensity of the C–D stretch would not be affected much by the neighboring atoms, i.e., they are essentially insensitive to the PAH size and structure as well as the presence of additional D atoms. Similarly, the frequency and intensity of the C–H stretch would also not be affected much by the presence of D atoms. The C–H and C–D stretches are expected to fall at very different frequencies due to the differences in mass and are not expected to mix, with the latter occurring at a wavelength longer by a factor of $\sim\sqrt{13/7}$.

3.2. Multideuterated Pyrene

We first consider the multideuterated species of pyrene which has a compact structure, and is the smallest parent molecule in our sample. We consider 288 isomers in total. The isomers for monodeuterated species $C_{16}H_9D$ (Pyre_1D) and dideuterated species $C_{16}H_8D_2$ (Pyre_2D) are shown in Figure 2, while $C_{16}H_7D_3$ (Pyre_3D), $C_{16}H_6D_4$ (Pyre_4D), and $C_{16}H_5D_5$ (Pyre_5D) are displayed in Figures 3–5, respectively. $C_{16}H_4D_6$ (Pyre_6D), $C_{16}H_3D_7$ (Pyre_7D), $C_{16}H_2D_8$ (Pyre_8D), and $C_{16}H_1D_9$ (Pyre_9D) are not shown since they are structurally identical to Pyre_4D, Pyre_3D, Pyre_2D, and Pyre_1D, respectively, when exchanging H with D.

For each isomer we compute its vibrational spectrum. We then obtain the mean spectrum for deuterated pyrenes of a given degree of deuteration (i.e., Pyre_nD) by averaging over all the isomers of Pyre_nD (see Figure 6). The frequencies are scaled with a factor of 0.9688 and each band is assigned a line width of 4 cm^{-1}.

To explore the effects of ionization on the spectra and band strengths of deuterated pyrenes, we also calculate the vibrational spectra of all the 288 isomers for deuterated pyrene cations ($Pyre\_nD^+$). The mean spectrum for each deuteration is shown in Figure 7.

Figures 6 and 7 clearly demonstrate that, upon deuteration, the vibrational spectra of both neutral and cationic pyrenes exhibit a new band at ~4.4 μm or ~2270 cm^{-1} attributed to C–D stretch, which is absent in the spectra of pure pyrene and its cation. The C–D in-plane (~11.7 μm) and oop bending (~15.4 μm) bands are also present (and their frequencies and intensities can be read from the Gaussian09 output files), but are difficult to identify in Figures 6 and 7 since they are mixed with the C–H oop bending bands and the C–C–C skeleton vibrational bands (see Hudgins et al. 2004).

As expected, Figures 6 and 7 also clearly show that, as the deuteration increases, the C–D stretch becomes stronger, while the C–H stretch at 3.3 μm weakens appreciably. The latter is due to the reduction in the number of C–H bonds as pyrene becomes more deuterated.

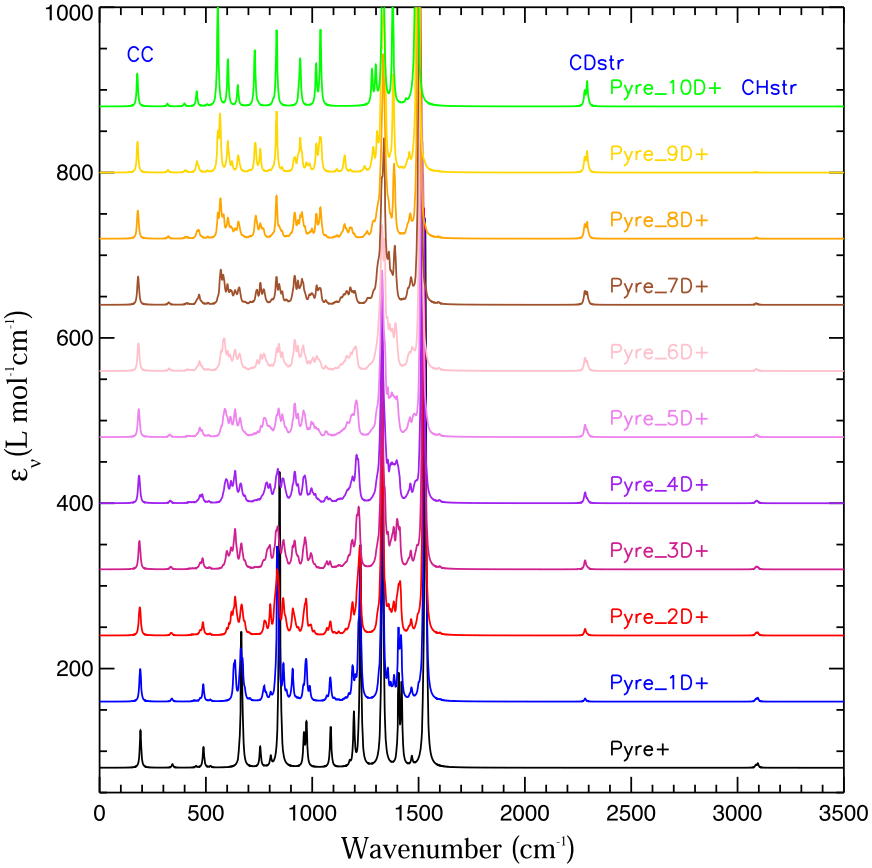

Figure 7. Same as Figure 6 but for deuterated pyrene cations.

By comparing Figure 7 with Figure 6, one immediately sees that, in comparison with their neutral counterparts, both the C–D and C–H stretches are substantially suppressed while the C–C stretches are considerably enhanced in cations. Such suppression in C–H stretches and enhancement in C–C stretches have also been seen in pure PAHs (e.g., see Allamandola et al. 1999 and Hudgins & Allamandola 2005), monodeuterated PAHs (Yang et al. 2020b), superhydrogenated PAHs (Yang et al. 2020a), and PAHs with aliphatic functional groups (Yang et al. 2017). Moreover, the C–D and C–H stretches of cationic species appear to occur at a somewhat shorter wavelength compared with their neutral counterparts.

As mentioned earlier in this section, while the C–D in-plane and oop bending bands of multideuterated pyrenes often blend with other bands, the C–D and C–H stretches lie in such a "clean" spectral region that we can unambiguously determine their frequencies and intensities. In the following we will focus on the 3.3 μm C–H stretch and the 4.4 μm C–D stretch. We obtain from DFT computations the intensities of the C–H and C–D stretches for all the 288 isomers of deuterated pyrenes. Let $A_{3.3}$ and $A_{4.4}$, respectively, be the intrinsic band strengths of the aromatic C–H and C–D stretches on a per-bond basis. We show in Figures 8 and 9 the intensities ($A_{3.3}$, $A_{4.4}$) and their ratios (i.e., $A_{4.4}/A_{3.3}$) for all the 288 isomers of deuterated pyrenes and their cations, respectively. In Tables 1, 2 we tabulate the *mean* wavelengths and intensities of the C–H and C–D stretches for each deuteration n (i.e., Pyre_nD and Pyre_nD$^+$, with $n = 0$, 1, 2, ..., 10), obtained by averaging over all the isomers of a given deuteration n.

The standard deviations for the mean wavelengths of the C–H and C–D stretches are very small for both neutral and cationic species, indicating that the central wavelengths of these two vibrational modes are very similar for different deuterations. By averaging over all deuterations, we obtain the mean band strengths $\langle A_{3.3}\rangle \approx 14.08 \pm 1.18$ km mol^{-1}, $\langle A_{4.4}\rangle \approx 7.63 \pm 0.79$ km mol^{-1}, and $\langle A_{4.4}/A_{3.3}\rangle \approx 0.55 \pm 0.09$ for neutral pyrenes, and $\langle A_{3.3}\rangle \approx 0.24 \pm 0.04$ km mol^{-1}, $\langle A_{4.4}\rangle \approx 1.42 \pm 0.26$ km mol^{-1}, and $\langle A_{4.4}/A_{3.3}\rangle \approx 6.42 \pm 3.45$ for cationic pyrenes. It is interesting to note that, overall, the band strengths of the C–H and C–D stretches of multideuterated pyrenes and their cations vary little with deuteration, although the band ratios $\langle A_{4.4}/A_{3.3}\rangle$ of pyrene cations exhibit a relatively larger scatter.

3.3. Multideuterated Perylene, Coronene and Ovalene

To explore the effects of PAH size on the band strengths of the C–H and C–D stretches, we now consider the multideuterated derivatives of three compact molecules which all are larger than the four-ring pyrene (see Section 3.2): the five-ring perylene, the seven-ring coronene, and the 10-ring ovalene (see Figure 1). Multideuterated perylene and ovalene have a huge number of isomers and it is impractical to compute the vibrational spectra of all their isomers. Therefore, 1072 isomers of perylene and 2462 isomers of ovalene are randomly selected for DFT computations. For coronene, we consider all of the 382 isomers of its multideuterated derivatives since it is highly symmetric and does not have as many "inequivalent" isomers as perylene and ovalene. As demonstrated in Section 3.2 and in

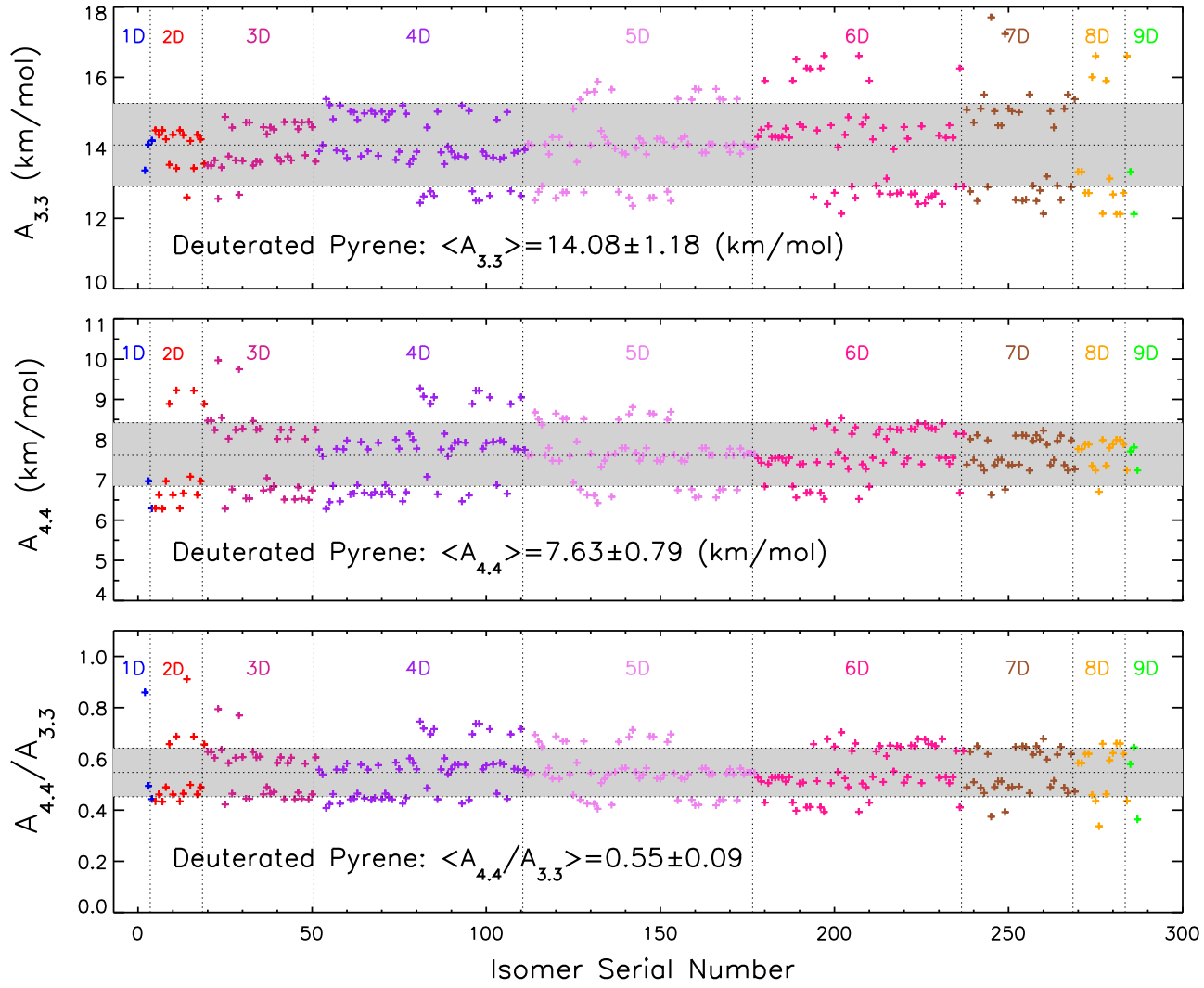

Figure 8. Band strengths of the 3.3 μm C–H stretches ($A_{3.3}$) and the 4.4 μm C–D stretches ($A_{4.4}$) as well as the band-strength ratios $A_{4.4}/A_{3.3}$ computed at level B3LYP/6-311+G** for all the 288 isomers of deuterated pyrenes (Pyre_nD) with different deuterations (i.e., n = 1, 2, ..., 9). Perdeuterated (n = 10) isomers are not shown since they do not have any C–H stretches.

Yang et al. (2020b), the 4.4 μm C–D stretch is substantially suppressed in deuterated PAH cations, and in the following we will only consider neutral species since the 4.4 μm C–D band seen in astrophysical regions is expected to predominantly arise from deuterated neutral PAHs.

In Figures 10–12 we show the mean vibrational spectra of a given deuteration n for multideuterated perylenes (Pery_nD), coronenes (Coro_nD), and ovalenes (Oval_nD), respectively. Just like that of multideuterated pyrenes, the C–D stretch is clearly seen at ~4.4 μm (~2250 cm^{-1}) in the computed spectra of all deuterated species. Also, the C–D stretch becomes appreciably stronger while the C–H stretch at 3.3 μm (~3000 cm^{-1}) weakens as the deuteration increases. Again, the C–D in-plane (~850 cm^{-1}) and oop bending modes (~650 cm^{-1}) are well mixed with the C–H oop bending modes and the C–C–C skeleton vibrational modes, and therefore they cannot be clearly identified in the mean spectra. Meanwhile, the intensities of the weak bands at $\lambda^{-1} \lesssim 400\,\mathrm{cm}^{-1}$, which arise from the C–C–C skeleton vibrations, are basically unaffected by deuteration, while their frequencies tend to be redshifted as deuteration increases.

In Figures 13–15 we show the intensities of the C–H stretch ($A_{3.3}$), the C–D stretch ($A_{4.4}$), and their ratios ($A_{4.4}/A_{3.3}$) for all the isomers of Pery_nD, Coro_nD, and Oval_nD of all possible deuterations, respectively (i.e., n ranges from 1 all the way to 12 for perylene, 12 for coronene, and 14 for ovalene). The overall mean wavelengths and intensities of the C–H and C–D stretches obtained by averaging over all the deuterations, as well as those of each deuteration n, are tabulated in Tables 3–5 for Pery_nD, Coro_nD, and Oval_nD, respectively. It is apparent that both the wavelengths and the intensities of the C–H and C–D stretches (on a per-unit-bond basis) are closely similar among deuterated species of different deuterations. While the intensities of the C–H and C–D stretches of Coro_nD and Oval_nD seem to exceed that of pyrene and perylene (as well as tetracene, see Section 3.4) by ~30%, their $A_{4.4}/A_{3.3}$ ratios are rather similar to that of the deuterated derivatives of pyrene, perylene, and tetracene.

3.4. Multideuterated Tetracene

In previous subsections, the molecules considered so far (i.e., pyrene, perylene, coronene, and ovalene) are all compact and pericondensed. To explore the effects of the molecular structures or shapes on the intrinsic strengths of the C–H and C–D stretches, we consider tetracene ($C_{18}H_{12}$), a linear,

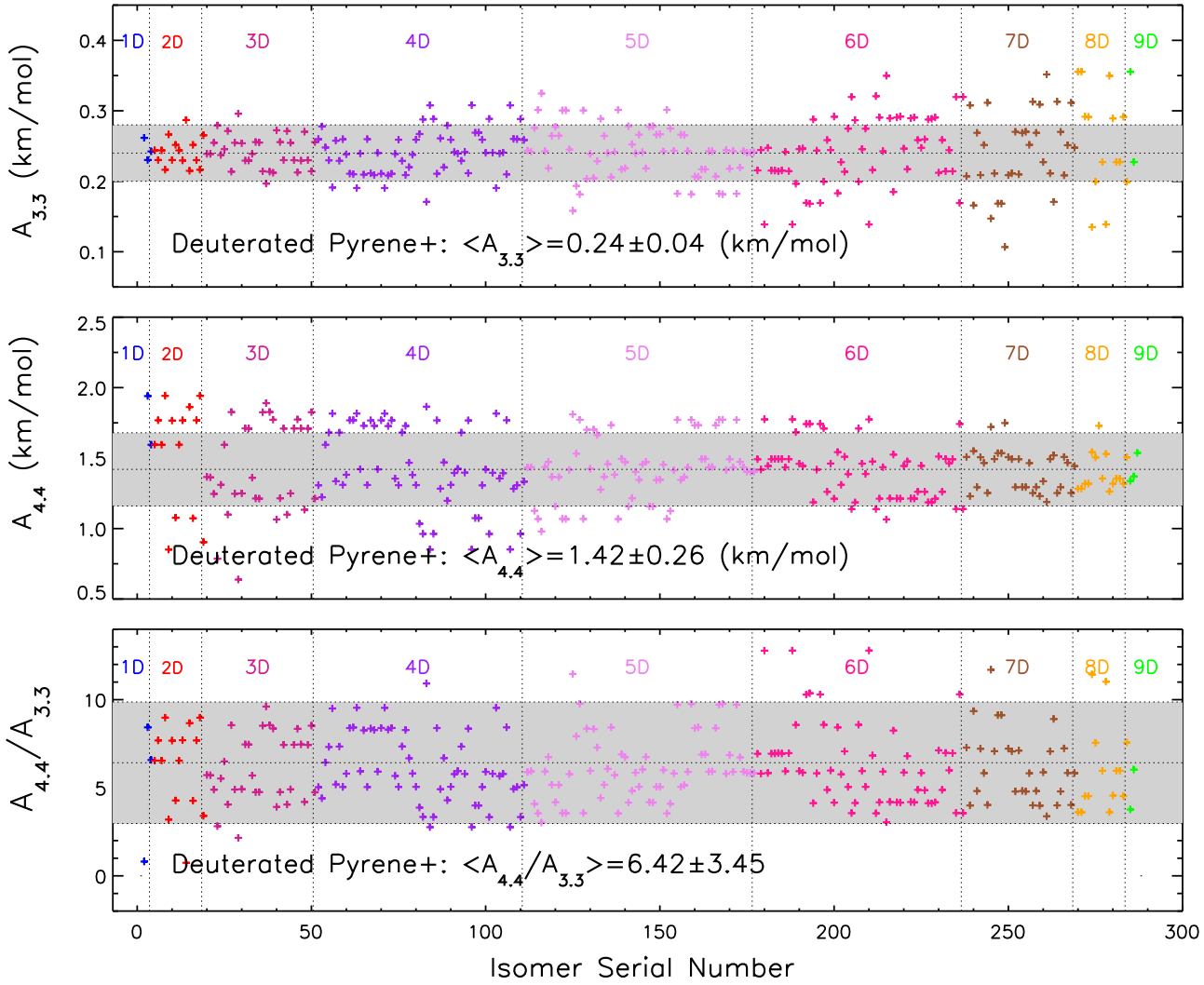

Figure 9. Same as Figure 8 but for deuterated pyrene cations.

Table 1
Wavelengths (λ) and Intensities (A_λ) of the Nominal "3.3 μm" C–H Stretch and "4.4 μm" C–D Stretch Computed at the B3LYP/6-311+G** Level for Deuterated Pyrenes of Different Deuterations

Compound	$\lambda_{3.3}$ (μm)	$A_{3.3}$ (km mol^{-1})	$\lambda_{4.4}$ (μm)	$A_{4.4}$ (km mol^{-1})	$A_{4.4}/A_{3.3}$
Pyre	3.25	13.97	…	…	…
Pyre_1D	3.25	13.88	4.41	8.24	0.60
Pyre_2D	3.25	14.01	4.40	7.61	0.55
Pyre_3D	3.25	14.00	4.40	7.65	0.55
Pyre_4D	3.25	14.05	4.40	7.62	0.55
Pyre_5D	3.25	14.07	4.40	7.63	0.55
Pyre_6D	3.25	14.09	4.40	7.63	0.55
Pyre_7D	3.26	14.17	4.39	7.62	0.55
Pyre_8D	3.26	14.13	4.39	7.65	0.56
Pyre_9D	3.26	15.11	4.39	7.58	0.53
Pyre_10D	…	…	4.39	7.66	…
Average	3.26	14.08	4.40	7.63	0.55
Stdev	0.00	1.18	0.00	0.79	0.09

Note. For each deuteration, the wavelengths and band intensities are obtained by averaging over all the considered isomers.

Table 2
Same as Table 1 but for Deuterated Pyrene Cations

Compound	$\lambda_{3.3}$ (μm)	$A_{3.3}$ (km mol^{-1})	$\lambda_{4.4}$ (μm)	$A_{4.4}$ (km mol^{-1})	$A_{4.4}/A_{3.3}$
Pyre+	3.23	0.24	…	…	…
Pyre_1D+	3.23	0.24	4.37	1.25	5.27
Pyre_2D+	3.24	0.24	4.38	1.45	6.19
Pyre_3D+	3.24	0.24	4.38	1.43	6.06
Pyre_4D+	3.24	0.24	4.38	1.43	6.18
Pyre_5D+	3.24	0.24	4.37	1.42	6.17
Pyre_6D+	3.24	0.24	4.37	1.41	6.31
Pyre_7D+	3.24	0.24	4.37	1.41	6.48
Pyre_8D+	3.24	0.24	4.37	1.40	8.33
Pyre_9D+	3.23	0.21	4.37	1.41	15.26
Pyre_10D+	…	…	4.37	1.38	…
Average	3.24	0.24	4.38	1.42	6.42
Stdev	0.00	0.04	0.00	0.26	3.45

catacondensed molecule (see Figure 1), as an extreme case, even though catacondensed molecules are less likely to survive in the hostile ISM.

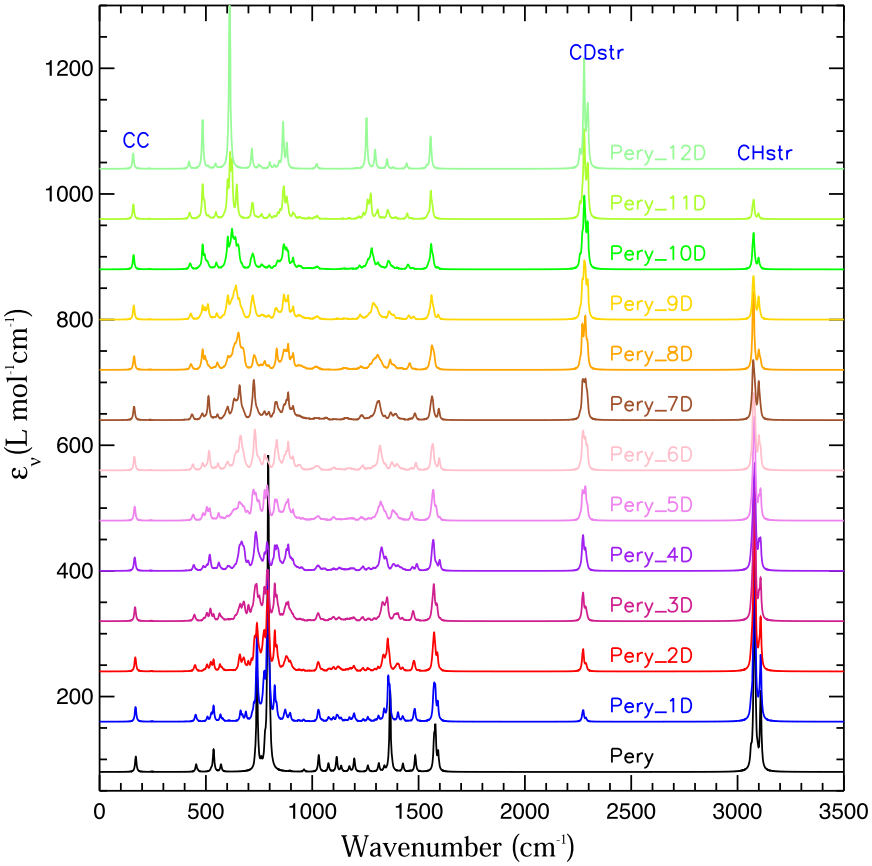

Figure 10. Same as Figure 6 but for deuterated perylenes.

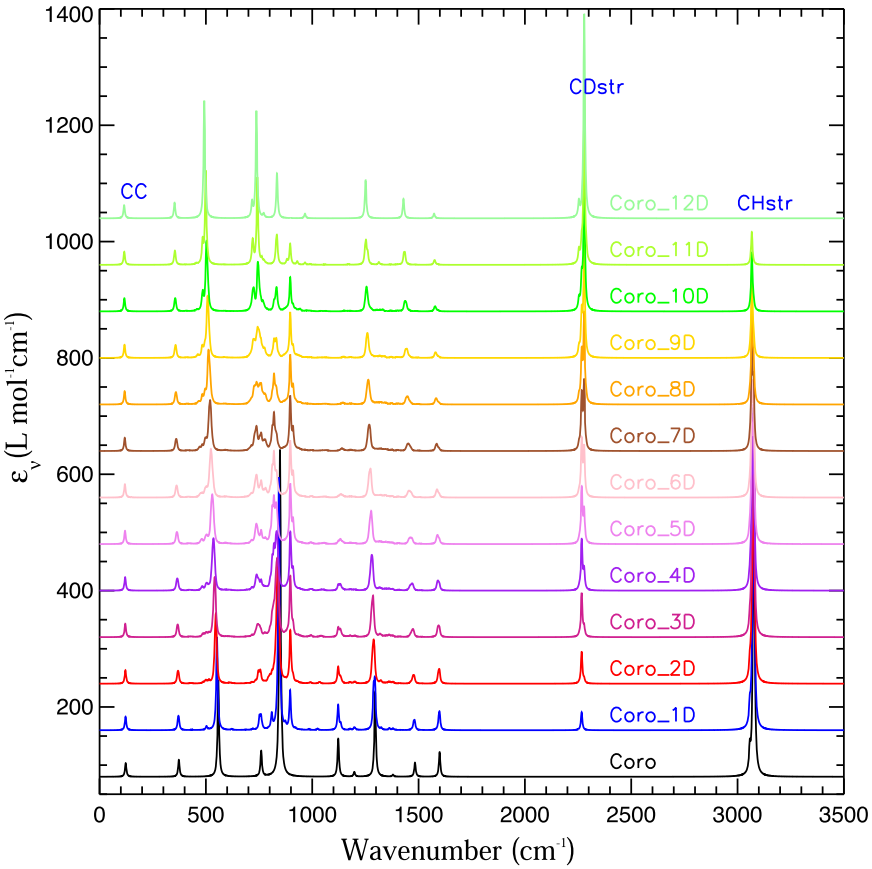

Figure 11. Same as Figure 6 but for deuterated coronenes.

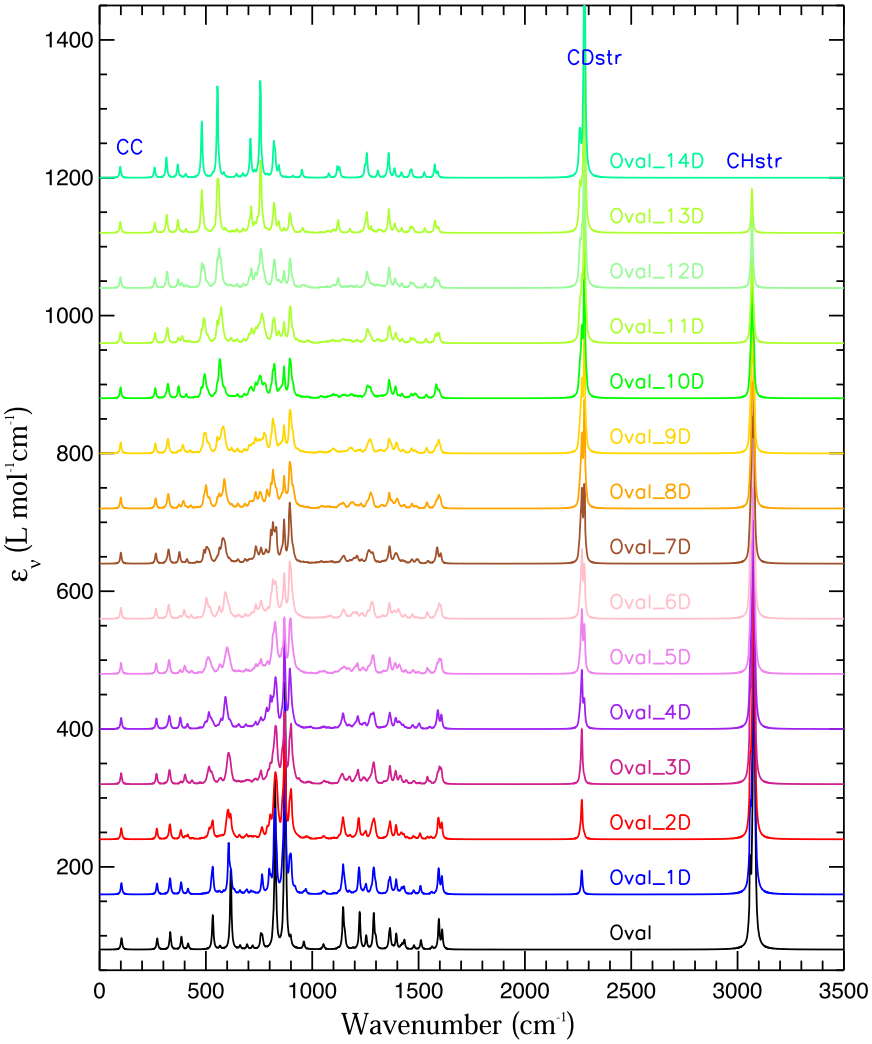

Figure 12. Same as Figure 6 but for deuterated ovalenes.

Similar to multideuterated perylenes and ovalenes, multideuterated tetracenes have too many isomers to be computationally manageable. Therefore, we randomly select 1072 isomers and compute their vibrational spectra. In Figure 16 we show the mean spectra of all the 12 deuterations of tetracene (i.e., Tetr_*n*D, where $n = 1, 2, ..., 12$). Again, the 4.4 μm C–D stretch is present in the computed spectra of all the isomers and becomes more pronounced as the molecule becomes more deuterated. It is worth noting that, compared with that of the deuterated derivatives of compact species (i.e., pyrene, perylene, coronene, and ovalene), the C–C–C skeleton vibrations at $\lambda^{-1} \lesssim 400\,\mathrm{cm}^{-1}$ are considerably suppressed in deuterated tetracenes. The mean intensities of the C–H and C–D stretches obtained by averaging over all the isomers of a given deuteration n are tabulated in Table 6. Also tabulated are the overall mean intensities averaged over all the deuterations. Figure 17 shows the intrinsic band strengths of the C–H and C–D stretches and their ratios ($A_{4.4}/A_{3.3}$) computed for all the 1072 isomers of deuterated tetracenes. It is apparent that both the mean band strengths $A_{3.3}$ and $A_{4.4}$ as well as $A_{4.4}/A_{3.3}$ of deuterated tetracenes do not vary much with deuteration and are closely consistent with that of multideuterated pyrenes and perylenes as well as monodeuterated species (see Yang et al. 2020b). This demonstrates that the intrinsic band strengths $A_{3.3}$ and $A_{4.4}$ and their ratios $A_{4.4}/A_{3.3}$ of deuterated species do not seem to exhibit any appreciable variations with the molecular structures of PAHs.

4. Discussion and Astrophysical Implications

As shown in Sections 3.2–3.4, the intrinsic band strengths of the C–H ($A_{3.3}$) and C–D ($A_{4.4}$) stretches, and particularly their ratios ($A_{4.4}/A_{3.3}$), vary very little with the degree of deuteration and the size and structure of the parent molecule, just as expected from the BO approximation, one of the foundations of the B3LYP DFT (see Section 3.1). Also, the wavelengths of the C–H and C–D stretches peak at 3.25 ± 0.1 μm and 4.40 ± 0.1 μm, respectively, and exhibit very little variations with the degree of deuteration and the size and structure of the parent molecule (see Tables 1–6), which is also expected from the BO approximation. As a matter of fact, previous DFT calculations on the vibrational spectra of pure PAHs of various sizes and structures (e.g., see Bauschlicher et al. 2008, 2009, 2018; Mattioda et al. 2020) have shown that the wavelengths and intensities of the C–H stretches are insensitive to the PAH size and structure. This is also true for the aromatic C–H stretches of PAHs attached with aliphatic side groups (e.g., see Yang et al. 2013, 2016). These can all be understood in the context of the BO approximation.

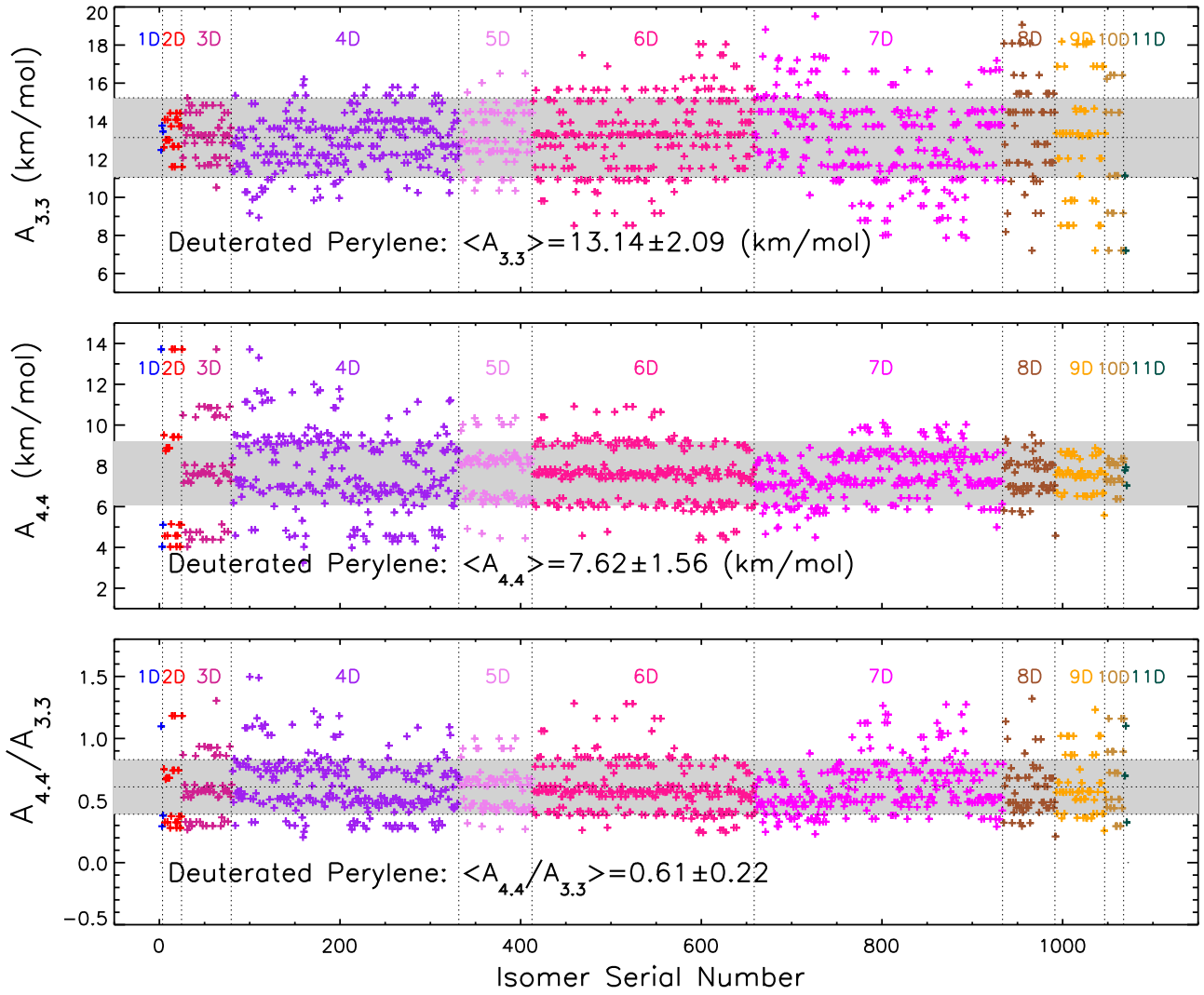

Figure 13. Same as Figure 8 but for deuterated perylenes.

We should note that, as shown in Tables 1–6, the C–H stretches of deuterated PAHs peak at ∼3.25 μm, which is appreciably shorter than the nominal 3.3 μm UIE band which typically occurs at ∼3.28–3.30 μm. Such a wavelength mismatch had been long noted by Sakata et al. (1990) and Kwok & Zhang (2013) for *pure* PAH molecules of which the C–H stretches lie shortward of the observed wavelength. Perhaps the wavelength mismatch could be accounted for by PAHs including substituents (e.g., N in place of C; see Hudgins et al. 2005; Mattioda et al. 2008) or superhydrogenation (Bernstein et al. 1996; Thrower et al. 2012; Sandford et al. 2013; Cruz-Diaz et al. 2020; Yang et al. 2020a). It is well recognized that upon substitution, the central wavelengths of the C–C and C–H bands of PAHs appreciably shift. Indeed, the observed subtle variations in the peak wavelength of the 6.2 μm C–C stretching emission band were commonly attributed to polycyclic aromatic nitrogen heterocycles—PAHs with one or more nitrogen atoms substituted into their carbon skeleton (see Hudgins et al. 2005). Also, both experimental measurements and DFT computations have shown that in superhydrogenated PAHs the wavelength of the C–H stretch shifts to longer wavelengths (see Sandford et al. 2013; Yang et al. 2020a).

By averaging the band strengths (on a per-unit-bond basis) over neutral PAHs of different deuteration, size, and structure, we obtain a recommended, mean band strength of $\langle A_{3.3}\rangle \approx 15.3 \pm 2.1\,\mathrm{km\,mol^{-1}}$ for the 3.3 μm C–H stretch, $\langle A_{4.4}\rangle \approx 8.5 \pm 1.0\,\mathrm{km\,mol^{-1}}$ for the 4.4 μm C–D stretch, and a band-strength ratio of $\langle A_{4.4}/A_{3.3}\rangle \approx 0.56 \pm 0.03$, which are closely similar to that of monodeuterated PAHs ($\langle A_{3.3}\rangle \approx 13.2 \pm 1.0\,\mathrm{km\,mol^{-1}}$, $\langle A_{3.3}\rangle \approx 7.3 \pm 2.4\,\mathrm{km\,mol^{-1}}$, and $\langle A_{4.4}/A_{3.3}\rangle \approx 0.56 \pm 0.19$).

Following Yang et al. (2020b), we define the degree of deuteration of a deuterated PAH molecule consisting of $N_{\rm H}$ H atoms and $N_{\rm D}$ D atoms as $[{\rm D/H}]_{\rm PAH} \equiv N_{\rm D}/(N_{\rm H}+N_{\rm D})$. Yang et al. (2020b) showed that one can derive $[{\rm D/H}]_{\rm PAH}$ from

$$[{\rm D/H}]_{\rm PAH} \approx \left\{1 + \left(\frac{I_{3.3}}{I_{4.4}}\right)_{\rm obs} \times \left(\frac{A_{4.4}}{A_{3.3}}\right) \times \left(\frac{B_{4.4}}{B_{3.3}}\right)\right\}^{-1}, \quad (1)$$

where $(I_{3.3}/I_{4.4})_{\rm obs}$ is the *observed* ratio of the power emitted from the 3.3 μm aromatic C–H band ($I_{3.3}$) to that from the 4.4 μm aromatic C–D band ($I_{4.4}$); $B_{3.3}$ and $B_{4.4}$ are the Planck functions at temperature T and wavelengths 3.3 μm and 4.4 μm, respectively, and $A_{3.3}$ and $A_{4.4}$ are the intrinsic band strengths of the aromatic C–H and C–D stretches (on a per C–H

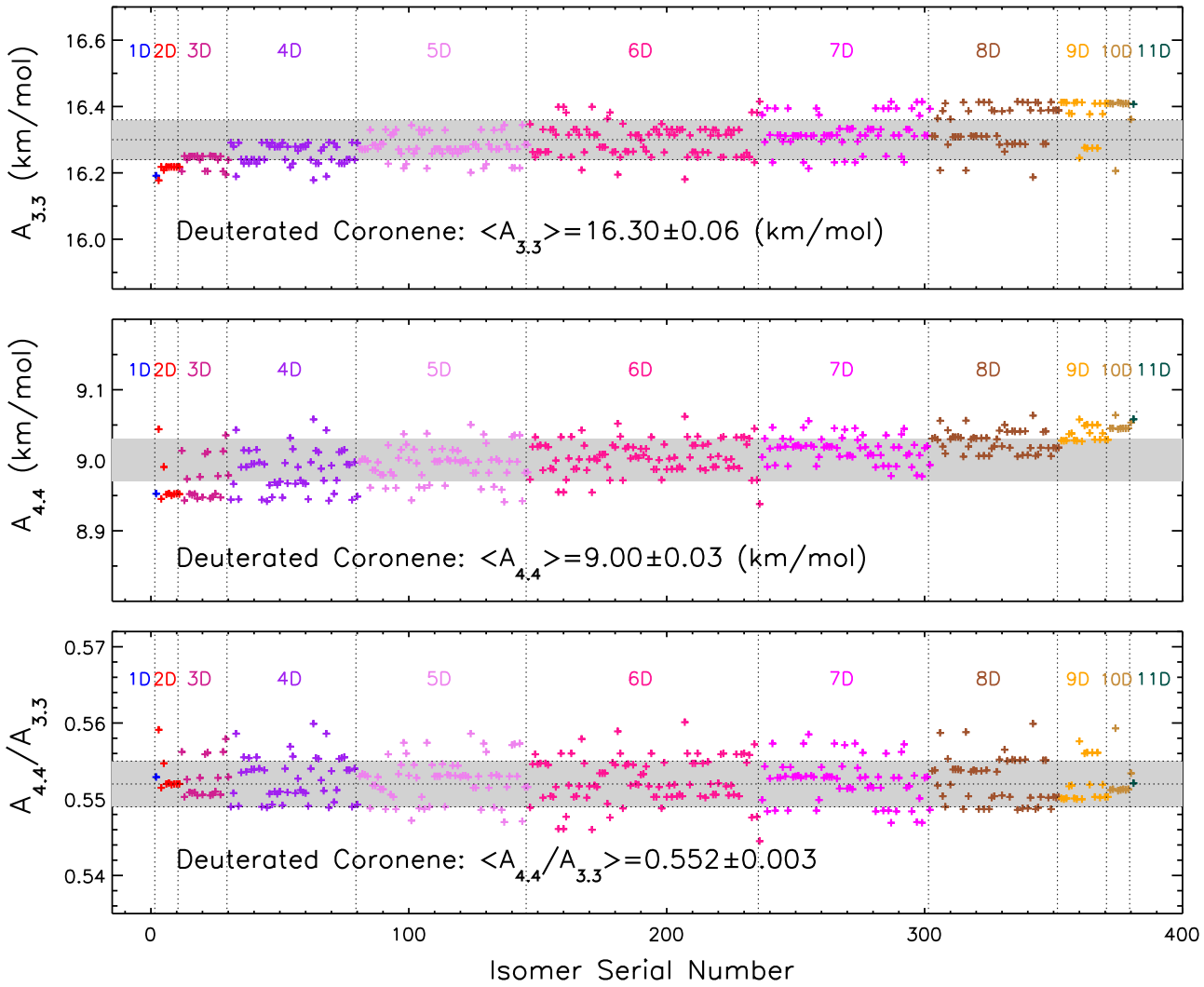

Figure 14. Same as Figure 8 but for deuterated coronenes.

or C–D bond basis), respectively. Yang et al. (2020b) have compiled all the available observational data on $(I_{3.3}/I_{4.4})_{\rm obs}$ (Peeters et al. 2004; Onaka et al. 2014; Doney et al. 2016) and obtained a mean value of $\langle (I_{3.3}/I_{4.4})_{\rm obs} \rangle \approx 52.6$. With $B_{3.3}/B_{4.4} \approx 0.70 \pm 0.28$ (suitable for $400 \lesssim T \lesssim 900$ K) and $A_{4.4}/A_{3.3} \approx 0.56$ for both monodeuterated species (Yang et al. 2020b) and multideuterated species (this work), we estimate $[{\rm D/H}]_{\rm PAH} \approx 2.4\%$. Compared with the interstellar abundance of $[{\rm D/H}]_{\rm ISM} \gtrsim 20 \pm 1$ ppm (see Section 1), this implies a D enrichment of a factor of ~1200 in PAHs.

Finally, it is rather puzzling to note that astronomical observations appear to show that whenever the 4.4 μm aromatic C–D band was detected, an accompanying aliphatic C–D band was also present. The latter is often stronger than the former by a factor of ~2–7 (Peeters et al. 2004; Doney et al. 2016), suggesting that a significant number of D atoms may be attached to aliphatic C atoms. While the deuteration of PAHs often requires UV photons to first rupture the C–H bond (e.g., see Allamandola et al. 1989), the attachment of aliphatic side groups (whether D-substituted or not) often occurs in benign environments (e.g., see Yang et al. 2017). Therefore, it is difficult to understand how PAHs could be both deuterated and attached with D-substituted aliphatic side groups. One possibility may be that, in dense molecular clouds, UV photolysis of PAHs in D-enriched ices might lead to deuteration (i.e., replacing H by D to form aromatic C–D bonds) *and* "superdeuteration" (i.e., one H atom and one D atom sharing a single C atom to form aliphatic C–H and C–D bonds; e.g., see Bernstein et al. 1999; Sandford et al. 2000). Future experimental and theoretical efforts are needed for solving this puzzle. More importantly, future high-signal-to-noise observations by the James Webb Space Telescope will provide valuable observational constraints on the aromatic and aliphatic C–D emission.

5. Summary

To facilitate a quantitative understanding of PAHs as a possible reservoir of interstellar D, we have employed the hybrid DFT method B3LYP in conjunction with the 6-311+G** basis set to calculate the vibrational spectra of deuterated PAHs of different deuterations, sizes, and structures (from pericondensed pyrene, perylene, coronene, and ovalene to linear catacondensed tetracene). It is found that the intrinsic band strengths of the 3.3 μm aromatic C–H stretch ($A_{3.3}$) and the 4.4 μm aromatic C–D stretch ($A_{4.4}$) as well as the band-strength ratios $A_{4.4}/A_{3.3}$, do not

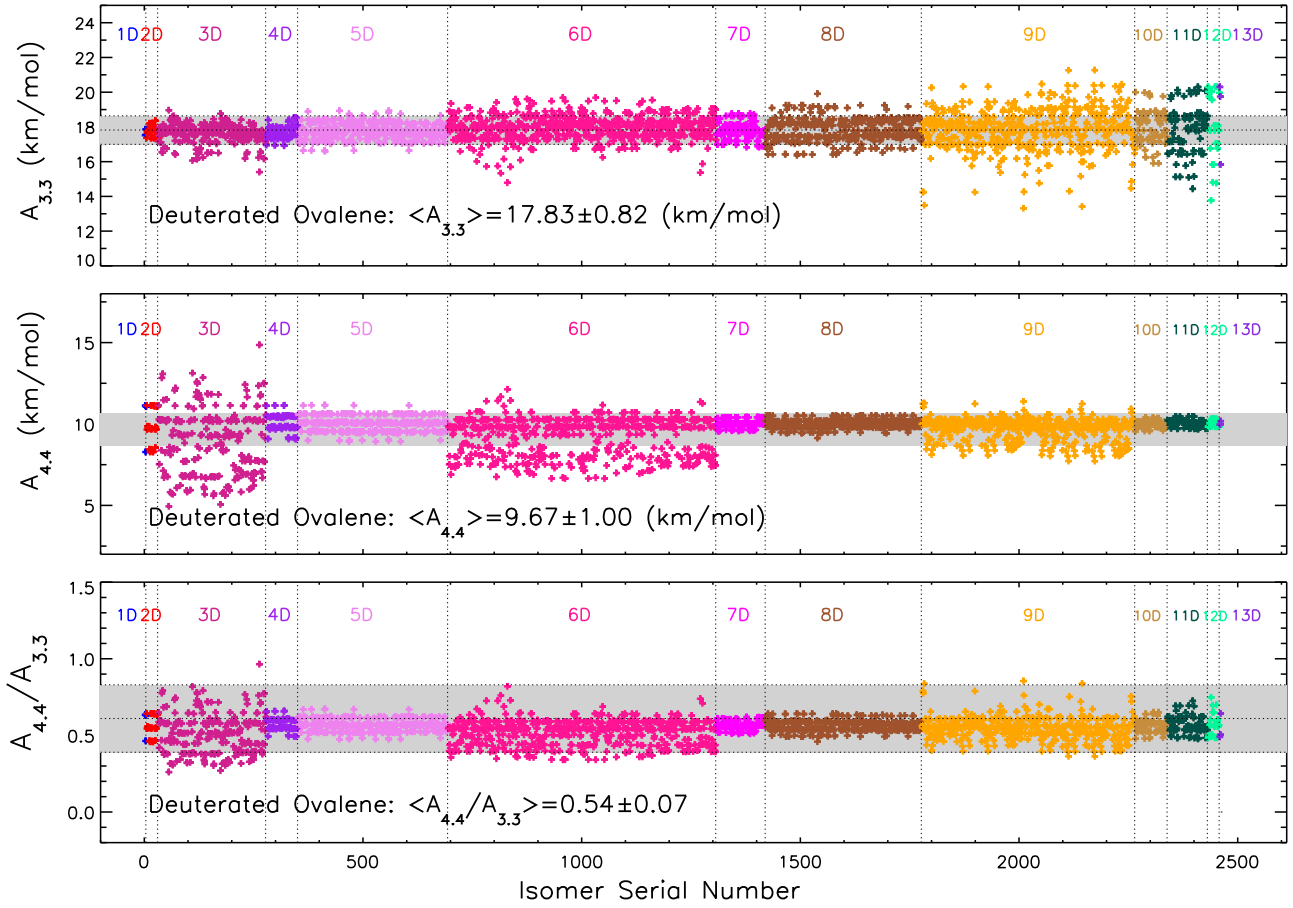

Figure 15. Same as Figure 8 but for deuterated ovalenes.

Table 3
Same as Table 1 but for Deuterated Perylenes

Compound	$\lambda_{3.3}$ (μm)	$A_{3.3}$ (km mol^{-1})	$\lambda_{4.4}$ (μm)	$A_{4.4}$ (km mol^{-1})	$A_{4.4}/A_{3.3}$
Pery	3.24	13.23	…	…	…
Pery_1D	3.24	13.24	4.39	7.62	0.59
Pery_2D	3.24	13.25	4.39	7.62	0.60
Pery_3D	3.24	13.26	4.39	7.61	0.59
Pery_4D	3.24	12.89	4.39	7.75	0.63
Pery_5D	3.24	13.22	4.39	7.62	0.59
Pery_6D	3.24	13.29	4.39	7.60	0.60
Pery_7D	3.24	13.04	4.39	7.56	0.61
Pery_8D	3.24	13.64	4.39	7.43	0.59
Pery_9D	3.24	13.32	4.39	7.59	0.62
Pery_10D	3.24	13.34	4.39	7.58	0.66
Pery_11D	3.24	13.35	4.39	7.58	0.71
Pery_12D	…	…	4.39	7.58	…
Average	3.24	13.14	4.39	7.62	0.61
Stdev	0.00	2.09	0.01	1.56	0.22

Table 4
Same as Table 1 but for Deuterated Coronenes

Compound	$\lambda_{3.3}$ (μm)	$A_{3.3}$ (km mol^{-1})	$\lambda_{4.4}$ (μm)	$A_{4.4}$ (km mol^{-1})	$A_{4.4}/A_{3.3}$
Coro	3.26	16.17	…	…	…
Coro_1D	3.26	16.19	4.41	8.95	0.55
Coro_2D	3.26	16.21	4.41	8.97	0.55
Coro_3D	3.26	16.24	4.41	8.97	0.55
Coro_4D	3.26	16.26	4.41	8.98	0.55
Coro_5D	3.26	16.28	4.41	8.99	0.55
Coro_6D	3.26	16.30	4.41	9.00	0.55
Coro_7D	3.26	16.32	4.41	9.02	0.55
Coro_8D	3.26	16.34	4.41	9.03	0.55
Coro_9D	3.26	16.37	4.41	9.04	0.55
Coro_10D	3.26	16.38	4.41	9.05	0.55
Coro_11D	3.26	16.41	4.41	9.06	0.55
Coro_12D	…	…	4.41	9.07	…
Average	3.26	16.30	4.41	9.00	0.55
Stdev	0.00	0.06	0.00	0.03	0.00

vary much among PAHs of different deuterations, sizes, and structures. By averaging over all these (neutral) molecules, we have determined the mean band strengths to be $\langle A_{3.3}\rangle \approx 15.3 \pm 2.1$ km mol^{-1} and $\langle A_{4.4}\rangle \approx 8.5 \pm 1.0$ km mol^{-1}. Since the mean band-strength ratio of $\langle A_{4.4}/A_{3.3}\rangle \approx 0.56 \pm 0.03$ for *multi-deuterated* PAHs is closely similar to that of *monodeuterated* PAHs, we conclude that the degree of deuteration of $[D/H]_{PAH} \approx 2.4\%$ *previously* estimated from the observed C–D to C–H intensity ratio based on the band-strength ratio of monodeuterated PAHs is robust. Finally, to investigate the charge effect on the band strengths, we have also calculated the vibrational spectra of multideuterated pyrene cations and found that, similar to monodeuterated PAHs, the C–H and C–D stretches are substantially suppressed in cations.

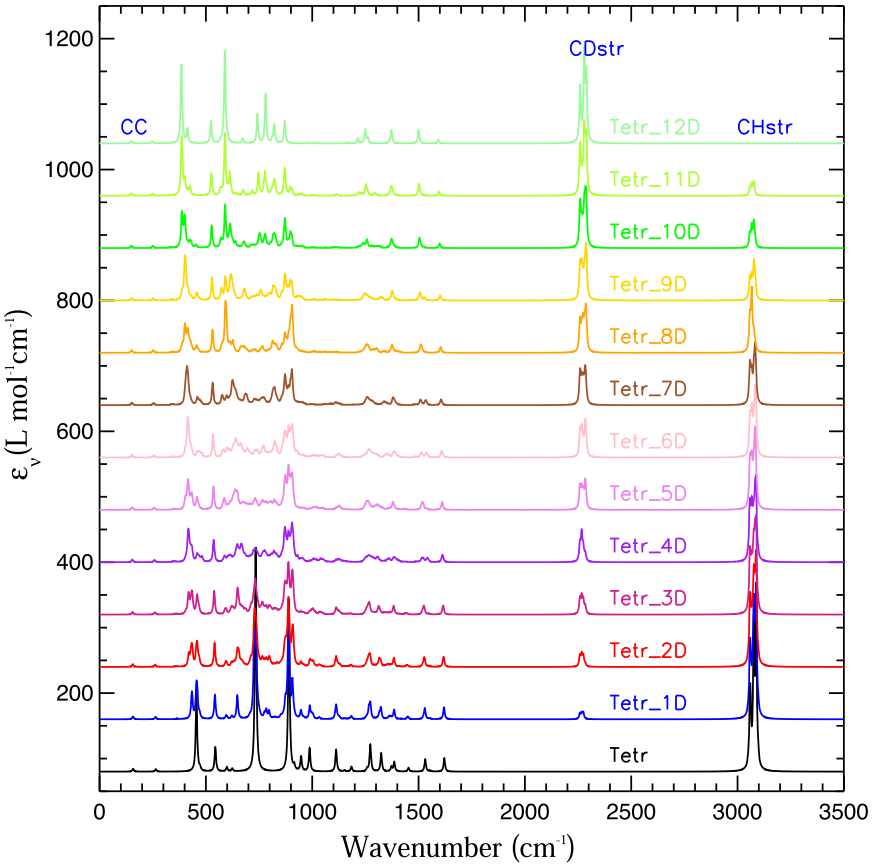

Figure 16. Same as Figure 6 but for deuterated tetracenes.

Table 5
Same as Table 1 but for Deuterated Ovalenes

Compound	$\lambda_{3.3}$ (μm)	$A_{3.3}$ (km mol^{-1})	$\lambda_{4.4}$ (μm)	$A_{4.4}$ (km mol^{-1})	$A_{4.4}/A_{3.3}$
Oval	3.26	17.68	…	…	…
Oval_1D	3.26	17.65	4.41	10.16	0.58
Oval_2D	3.26	17.73	4.41	9.90	0.56
Oval_3D	3.26	17.59	4.41	8.94	0.51
Oval_4D	3.26	17.68	4.41	10.12	0.57
Oval_5D	3.26	17.76	4.41	10.00	0.56
Oval_6D	3.26	17.94	4.41	9.30	0.52
Oval_7D	3.26	17.78	4.41	10.03	0.56
Oval_8D	3.26	17.82	4.41	10.01	0.56
Oval_9D	3.26	17.87	4.41	9.73	0.55
Oval_10D	3.26	17.97	4.41	9.98	0.56
Oval_11D	3.26	17.84	4.41	10.04	0.57
Oval_12D	3.26	17.85	4.41	10.05	0.57
Oval_13D	3.26	18.63	4.41	10.04	0.55
Oval_14D	…	…	4.41	10.07	…
Average	3.26	17.83	4.41	9.67	0.55
Stdev	0.00	0.82	0.00	1.00	0.07

Table 6
Same as Table 1 but for Deuterated Tetracenes

Compound	$\lambda_{3.3}$ (μm)	$A_{3.3}$ (km mol^{-1})	$\lambda_{4.4}$ (μm)	$A_{4.4}$ (km mol^{-1})	$A_{4.4}/A_{3.3}$
Tetr	3.26	13.59	…	…	…
Tetr_1D	3.26	13.61	4.41	7.50	0.55
Tetr_2D	3.26	13.63	4.41	7.51	0.55
Tetr_3D	3.26	13.65	4.41	7.52	0.55
Tetr_4D	3.26	13.56	4.41	7.16	0.53
Tetr_5D	3.26	13.50	4.41	7.61	0.57
Tetr_6D	3.26	13.70	4.41	7.55	0.55
Tetr_7D	3.26	13.79	4.41	7.28	0.53
Tetr_8D	3.26	12.60	4.41	7.70	0.62
Tetr_9D	3.26	13.75	4.41	7.59	0.56
Tetr_10D	3.26	13.77	4.41	7.60	0.57
Tetr_11D	3.26	13.78	4.41	7.61	0.58
Tetr_12D	…	…	4.41	7.62	…
Average	3.26	13.64	4.41	7.40	0.55
Stdev	0.00	1.01	0.01	0.54	0.07

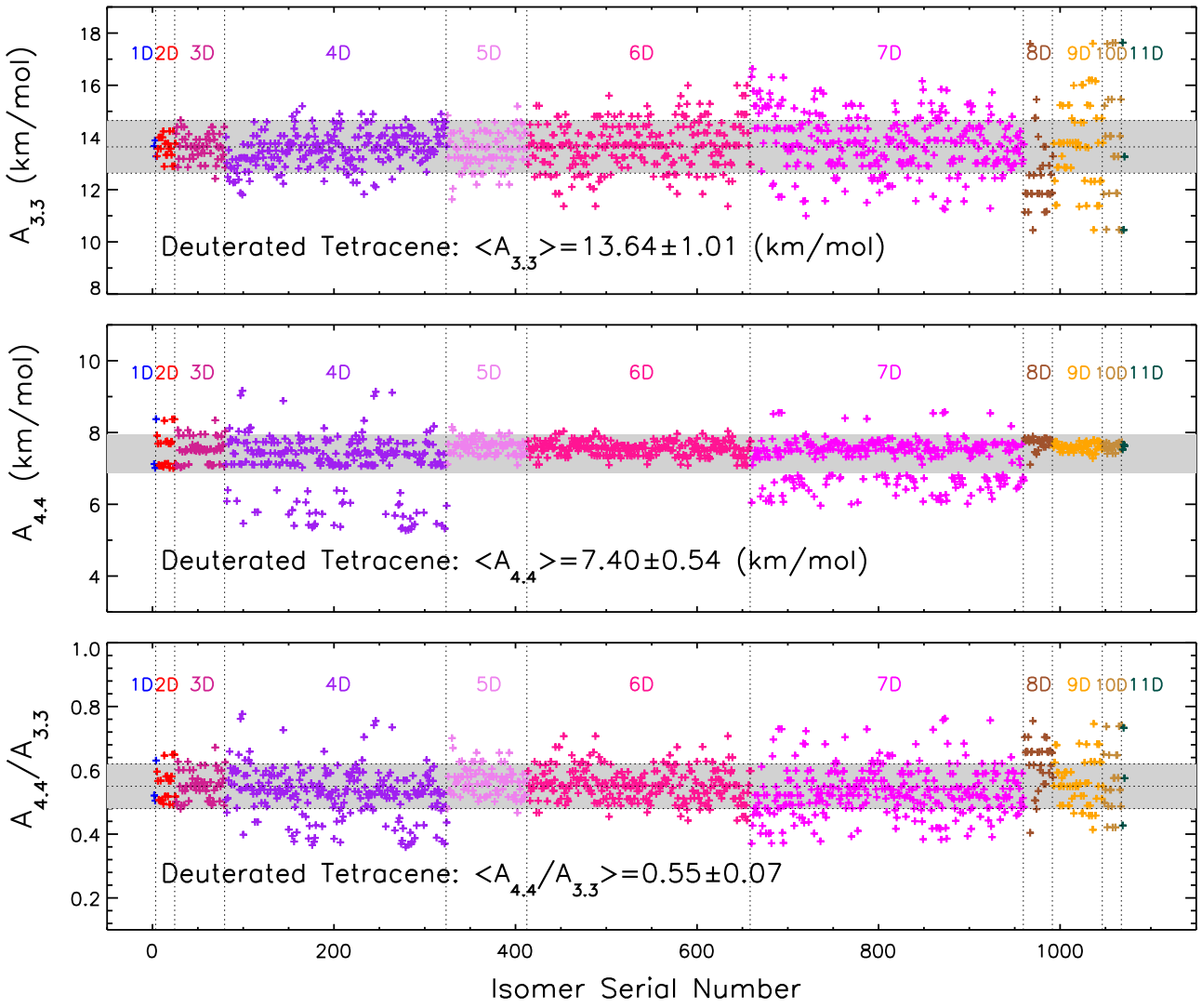

Figure 17. Same as Figure 8 but for deuterated tetracenes.

We thank B. T. Draine, Y. H. Li, A. N. Witt, and the anonymous referees for very helpful suggestions. X.J.Y. is supported in part by NSFC 11873041, 11473023, the CSST Milky Way Survey Dust and Extinction Project, and the NSFC-CAS Joint Research Funds in Astronomy (U1731106, U1731107). A.L. is supported in part by NASA grants 80NSSC19K0572 and 80NSSC19K0701. R.G. is supported in part by NSF-PRISM grant Mathematics and Life Sciences (0928053). Computations were performed using the high-performance computer resources of the University of Missouri Bioinformatics Consortium.

ORCID iDs

X. J. Yang https://orcid.org/0000-0002-6605-6512
Aigen Li https://orcid.org/0000-0002-1119-642X
R. Glaser https://orcid.org/0000-0003-3673-3858

References

Allamandola, L. J., Hudgins, D. M., & Sandford, S. A. 1999, ApJ, 511, 115
Allamandola, L. J., Sandford, S. A., & Wopenka, B. 1987, Sci, 237, 56
Allamandola, L. J., Tielens, A. G. G. M., & Barker, J. R. 1989, ApJS, 71, 733
Allen, M. M., Jenkins, E. B., & Snow, T. P. 1992, ApJS, 83, 261
Bauschlicher, C. W., Langhoff, S. R., Sandford, S. A., & Hudgins, D. M. 1997, JPCA, 101, 2414
Bauschlicher, C. W., Peeters, E., & Allamandola, L. J. 2008, ApJ, 678, 316
Bauschlicher, C. W., Peeters, E., & Allamandola, L. J. 2009, ApJ, 697, 311
Bauschlicher, C. W., Ricca, A., Boersma, C., & Allamandola, L. J. 2018, ApJS, 234, 32
Bernstein, L. S., Shroll, R. M., Lynch, D. K., & Clark, F. O. 2017, ApJ, 836, 229
Bernstein, M. P., Sandford, S. A., & Allamandola, L. J. 1996, ApJL, 472, L127
Bernstein, M. P., Sandford, S. A., Allamandola, L. J., et al. 1999, Sci, 283, 1135
Boesgaard, A. M., & Steigman, G. 1985, ARA&A, 23, 319
Borowski, P. 2012, JPCA, 116, 3866
Buragohain, M., Pathak, A., Sakon, I., & Onaka, T. 2020, ApJ, 892, 11
Buragohain, M., Pathak, A., Sarre, P., Onaka, T., & Sakon, I. 2015, MNRAS, 454, 193
Buragohain, M., Pathak, A., Sarre, P., Onaka, T., & Sakon, I. 2016, P&SS, 133, 97
Cami, J. 2011, in EAS Publications Series 46, PAHs and the Universe: A Symp. to Celebrate the 25th Anniversary of the PAH Hypothesis, ed. C. Joblin & A. G. G. M. Tielens (Les Ulis: EDP Sciences), 117
Clemett, S. J., Maechling, C. R., Zare, R. N., Swan, P. D., & Walker, R. M. 1993, Sci, 262, 721
Coc, A., Vangioni-Flam, E., Descouvemont, P., Adahchour, A., & Angulo, C. 2004, ApJ, 600, 544
Cooke, R., Pettini, M., & Steidel, C. C. 2018, ApJ, 855, 102
Cruz-Diaz, G. A., Ricca, A., & Mattioda, A. L. 2020, ESC, 4, 1730

Doney, K. D., Candian, A., Mori, T., Onaka, T., & Tielens, A. G. G. M. 2016, A&A, 586, 65
Draine, B. T. 1990, in ASP Conf. Ser. 12, The Evolution of the Interstellar Medium, ed. L. Blitz (San Francisco, CA: ASP)
Draine, B. T. 2004, in Origin and Evolution of the Elements, ed. A. McWilliam & M. Rauch (Cambridge: Cambridge Univ. Press), 317
Draine, B. T. 2006, in ASP Conf. Ser. 348, Astrophysics in the Far Ultraviolet: Five Years of Discovery with FUSE, ed. G. Sonneborn, H. Moos, & B.-G. Andersson (San Francisco, CA: ASP), 58
Draine, B. T., & Li, A. 2007, ApJ, 657, 810
Draine, B. T., Li, A., Hensley, B. S., et al. 2020, ApJ, in press (arXiv:2011.07046)
Frisch, M. J., Trucks, G. W., Schlegel, H. B., et al. 2016, Gaussian 16, Revision C.01 (Wallingford, CT: Gaussian, Inc.)
Hudgins, D. M., & Allamandola, L. J. 2005, in IAU Symp. 231, Astrochemistry: Recent Successes and Current Challenges, ed. D. C. Lis, G. A. Blake, & E. Herbst (Cambridge: Cambridge Univ. Press), 443
Hudgins, D. M., Bauschlicher, C. W., Jr., & Allamandola, L. J. 2005, ApJ, 632, 316
Hudgins, D. M., Bauschlicher, C. W., Jr., & Sandford, S. A. 2004, ApJ, 614, 770
Hudgins, D. M., Sandford, S. A., & Allamandola, L. J. 1994, JPhCh, 98, 4243
Jenkins, E. B., Tripp, T. M., Wózniak, P., Sofia, U. J., & Sonneborn, G. 1999, ApJ, 520, 182
Kerridge, J. F., Chang, S., & Shipp, R. 1987, GeCoA, 51, 2527
Kwok, S., & Zhang, Y. 2011, Natur, 479, 80
Kwok, S., & Zhang, Y. 2013, ApJ, 771, 5
Li, A. 2020, NatAs, 4, 339
Li, A., & Draine, B. T. 2001, ApJ, 554, 778
Loinard, L., Castets, A., Ceccarelli, C., et al. 2000, A&A, 359, 1169
Mattioda, A. L., Hudgins, D. M., Boersma, C., et al. 2020, ApJS, 251, 22
Mattioda, A. L., Rutter, L., Parkhill, J., et al. 2008, ApJ, 680, 1243
Mazzitelli, I., & Moretti, M. 1980, ApJ, 235, 995
McGuire, B. A., Loomis, R. A., Burkhardt, A. M., et al. 2021, Sci, 371, 1265
McKee, C. 1989, in IAU Symp. 135, Interstellar Dust, ed. L. J. Allamandola & A. G. G. M. Tielens (Dordrecht: Kluwer), 431
Onaka, T., Mori, T. I., Sakon, I., et al. 2014, ApJ, 780, 114
Parise, B., Ceccarelli, C., Tielens, A. G. G. M., et al. 2002, A&A, 393, L49
Peeters, E., Allamandola, L. J., Bauschlicher, C. W., Jr., et al. 2004, ApJ, 604, 252
Prodanović, T., Steigman, G., & Fields, B. D. 2010, MNRAS, 406, 1108
Rosenberg, M. J. F., Berné, O., Boersma, C., Allamandola, L. J., & Tielens, A. G. G. M. 2011, A&A, 532, A128
Roueff, E., Tin, S., Coudert, L. H., et al. 2000, A&A, 354, L63
Sadjadi, S., Zhang, Y., & Kwok, S. 2017, ApJ, 845, 123
Sakata, A., Wada, S., Onaka, T., & Tokunaga, A. T. 1990, ApJ, 353, 543
Sánchez, A. G., Baugh, C. M., Percival, W. J., et al. 2006, MNRAS, 366, 189
Sandford, S. A., Bernstein, M. P., Allamandola, L. J., Gillette, J. S., & Zare, R. N. 2000, ApJ, 538, 691
Sandford, S. A., Bernstein, M. P., & Dworkin, J. P. 2001, M&PS, 36, 1117
Sandford, S. A., Bernstein, M. P., & Materese, C. K. 2013, ApJS, 205, 8
Shi, X., He, C, Pickard, C. J., Tang, C., & Zhong, J. 2018, PhRvB, 97, 014104
Spergel, D. N., Verde, L., Peiris, H. V., et al. 2003, ApJS, 148, 175
Thrower, J. D., Jørgensen, B., Friis, E. E., et al. 2012, ApJ, 752, 3
van der Tak, F. F. S., Schilke, P., Müuller, H. S. P., et al. 2002, A&A, 388, L53
Vastel, C., Phillips, T. G., Ceccarelli, C., & Pearson, J. 2003, ApJL, 593, L97
Wexler, A. S. 1967, ApSRv, 1, 29
Yang, X. J., Glaser, R., Li, A., & Zhong, J. X. 2013, ApJ, 776, 110
Yang, X. J., Glaser, R., Li, A., & Zhong, J. X. 2017, NewAR, 77, 1
Yang, X. J., Li, A., & Glaser, R. 2016, ApJ, 825, 22
Yang, X. J., Li, A., & Glaser, R. 2020a, ApJS, 247, 1
Yang, X. J., Li, A., & Glaser, R. 2020b, ApJS, 251, 12
Zavarygin, E. O., Webb, J. K., Riemer-Sørensen, S., & Dumont, V. 2018, MNRAS, 477, 5536
Zhang, Y., & Kwok, S. 2015, ApJ, 798, 37